Gauss-Seidel and Successive Overrelaxation Methods for Radiative Transfer with Partial Frequency Redistribution

M. Sampoorna[1] and J. Trujillo Bueno[1,2,3]

[1]*Instituto de Astrofísica de Canarias, E-38205 La Laguna, Tenerife, Spain*

[2]*Departamento de Astrofísica, Facultad de Física, Universidad de La Laguna, Tenerife, Spain*

[3]*Consejo Superior de Investigaciones Científicas, Spain*

Accepted in February 2010 for publication in The Astrophysical Journal

ABSTRACT

The linearly-polarized solar limb spectrum that is produced by scattering processes contains a wealth of information on the physical conditions and magnetic fields of the solar outer atmosphere, but the modeling of many of its strongest spectral lines requires solving an involved non-LTE radiative transfer problem accounting for partial redistribution (PRD) effects. Fast radiative transfer methods for the numerical solution of PRD problems are also needed for a proper treatment of hydrogen lines when aiming at realistic time-dependent magneto-hydrodynamic simulations of the solar chromosphere. Here we show how the two-level atom PRD problem with and without polarization can be solved accurately and efficiently via the application of highly convergent iterative schemes based on the Gauss-Seidel (GS) and Successive Overrelaxation (SOR) radiative transfer methods that had been previously developed for the complete redistribution (CRD) case. Of particular interest is the Symmetric SOR method, which allows us to reach the fully converged solution with an order of magnitude of improvement in the total computational time with respect to the Jacobi-based local ALI (Accelerated Lambda Iteration) method.

Subject headings: line : profiles – methods: numerical – polarization – radiative transfer – scattering – stars : atmospheres – Sun: atmosphere

1. Introduction

The phenomenon of scattering in a spectral line is a complicated physical process where partial correlations between the incoming and outgoing photons can occur (e.g., Mihalas

1978; Cannon 1985; Oxenius & Simonneau 1994). This happens when the shape of the incident spectrum that populates the upper level via radiative absorptions is not flat over the line. These partial redistribution (PRD) effects tend to be more important in strong lines, such as the solar Mg II and Ca II resonance lines and Lyman α. In particular, the wings of the intensity profiles of these lines are strongly affected by PRD effects, especially concerning observations close to the edge of the solar disk.

Only a small number of solar spectral lines show conspicuous PRD signatures in their emergent *intensity* profiles. However, a substantially larger fraction show clear hints of PRD effects in the fractional linear polarization Q/I profiles that result from scattering processes in quiet regions of the solar atmosphere (e.g., see the classification proposed by Belluzzi & Landi Degl'Innocenti 2009 of the various Q/I shapes found in the linearly-polarized solar limb spectrum observed by Stenflo & Keller 1997 and by Gandorfer 2000, 2002, 2005). To achieve a rigorous modeling of the weak polarization signals that constitute this so-called *Second Solar Spectrum* is very important, mainly because it contains valuable information on the magnetism of the extended solar atmosphere (e.g., the review by Trujillo Bueno 2009). To this end it is crucial to solve accurately and efficiently the non-LTE (Local Thermodynamic Equilibrium) radiative transfer problem of resonance line polarization taking into account PRD effects. The present paper represents a contribution towards this goal.

Fast iterative methods based on operator splitting were introduced to astrophysics by Cannon (1973) for unpolarized radiative transfer with complete redistribution (CRD) in scattering. Extensions of this type of methods to PRD were done by Vardavas & Cannon (1976), and later by Scharmer (1983) and Uitenbroek (2001). These methods are widely known today as Accelerated Lambda Iteration (ALI) methods (e.g., the review by Hubeny 2003). An optimum choice for the approximate lambda operator is the diagonal of the true lambda operator, which was introduced in the seminal paper by Olson, Auer & Buchler (1986). This Jacobi based method for solving the two-level atom problem with CRD was generalized by Paletou & Auer (1995, hereafter PA95) to unpolarized PRD radiative transfer.

Superior radiative transfer methods based on Gauss-Seidel (GS) and successive overrelaxation (SOR) iteration were developed by Trujillo Bueno & Fabiani Bendicho (1995, hereafter TF95). The convergence rate of these iterative schemes is equivalent to that corresponding to upper or lower triangular approximate lambda operators, but without the need of constructing and inverting such operators. Therefore, the computing time per iteration is similar to that of the Jacobi scheme or local ALI method, but the number of iterations needed to reach convergence is an order of magnitude smaller. In their paper, TF95 suggested the strategy to generalize their GS-based methods to the multilevel atom case. Fabiani Bendicho, Trujillo Bueno & Auer (1997) implemented such a MUltilevel GAuss Sei-

del method (MUGA; see also Fabiani Bendicho & Trujillo Bueno 1999 and Asensio Ramos & Trujillo Bueno 2006 for its generalization to 3D and spherical geometries) and combined it with a non-linear multigrid iterative scheme to produce multilevel radiative transfer programs whose convergence rates are insensitive to the grid size. Here we present the generalization of the GS and SOR radiative transfer methods of TF95 to the two-level atom PRD problem, with and without scattering polarization.

An alternative iterative scheme for solving radiative transfer problems is the preconditioned bi-conjugate gradient method (Castor 2004), which has been recently applied to plane-parallel (Paletou & Anterrieu 2009; Nagendra et al. 2009) and spherical geometries (Anusha et al. 2009). Its rate of convergence is similar to that of the optimal Symmetric SOR method of TF95 (see Castor 2004), but an efficient generalization of the preconditioned bi-conjugate gradient method to the multilevel atom case is presently an unsolved problem.

A suitable generalization of the local ALI method to the Zeeman line transfer problem was done by Trujillo Bueno & Landi Degl'Innocenti (1996). Extensions of the Jacobi, GS, and SOR schemes to scattering polarization were carried out by Faurobert-Scholl et al. (1997, CRD Jacobi), Paletou & Faurobert-Scholl (1997, PRD Jacobi), and Trujillo Bueno & Manso Sainz (1999, CRD Jacobi, GS and SOR). All these iterative schemes for non-LTE radiative transfer were generalized to solve CRD multi-level scattering polarization problems in the presence of a magnetic field, including the possibility of atomic polarization in all levels (Trujillo Bueno 1999; Manso Sainz & Trujillo Bueno 2003, see also Trujillo Bueno 2003). However only the Jacobi iterative scheme has been applied to solve the two-level atom polarized PRD radiative transfer problem in the presence of an external magnetic field (Nagendra et al. 1999; Fluri et al. 2003; Sampoorna et al. 2008, see also the reviews by Nagendra 2003; Nagendra & Sampoorna 2009). Here we extend the GS and SOR iterative methods to solve polarized PRD problems in the absence or in the presence of magnetic fields which do not break the axial symmetry of the problem (e.g., the micro-turbulent field case).

The accuracy of any iterative method for a given depth grid resolution is determined by the truncation error or the true error (see Auer, Fabiani Bendicho & Trujillo Bueno 1994). So far the study of the true error is limited to only CRD problems (e.g., Auer et al. 1994; TF95; Faurobert-Scholl et al. 1997; Trujillo Bueno & Manso Sainz 1999; Chevallier et al. 2003). Hence, in this paper we discuss certain aspects of the true error for PRD problems.

For our study we consider all the three angle-averaged (AA) redistribution functions of Hummer (1962), namely $R_{\rm I,II,III,AA}$, and the linear combination of $R_{\rm II,AA}$ and $R_{\rm III,AA}$. We recall that physically (1) $R_{\rm I,AA}$ represents the case of infinitely sharp lower and upper levels (or pure Doppler redistribution in the laboratory frame); (2) $R_{\rm II,AA}$ represents the case of infinitely sharp lower level and radiatively broadened upper level (coherent scattering in the

atomic frame); (3) $R_{\rm III,AA}$ represents the case of infinitely sharp lower level and radiatively as well as collisionally broadened upper level (CRD in the atomic frame).

The logical structure of this paper is the following: §§ 2, 3, and 4 are devoted to unpolarized PRD radiative transfer. We first recall the basic equations, the Jacobi scheme used by PA95 for $R_{\rm II,AA}$ redistribution, and then present briefly the extension of this scheme to $R_{\rm I,III,AA}$ redistributions. Next, we present the generalization of the GS and SOR schemes of TF95 to PRD. A detailed study of the true error for all the three iterative schemes with AA redistribution functions is conducted in § 4. §§ 5, 6, and 7 are devoted to polarized PRD radiative transfer. In § 5 we present the basic equations of polarized radiative transfer. Our generalization of the Jacobi, GS, and SOR schemes of § 3 to scattering polarization is presented in § 6. A detailed study of the true error for polarized PRD case is given in § 7. Concluding remarks are given in § 8.

2. Unpolarized PRD radiative transfer

We consider the case of scattering on a two-level atom with a background continuum. The scattering mechanism is described by the AA redistribution functions of Hummer (1962). Furthermore, we approximate the stellar atmosphere by a one-dimensional plane parallel slab of total optical thickness T. Under these assumptions, the scalar radiative transfer equation is given by

$$\frac{\mathrm{d}}{\mathrm{d}\tau} I_{x\mu}(\tau) = I_{x\mu}(\tau) - S_x(\tau), \tag{1}$$

where $I_{x\mu}(\tau)$ is the specific intensity, x is the frequency from line center in units of the Doppler width, $\mu = \cos\theta$, with θ being the angle between the ray and the atmospheric normal, and the optical depth τ is defined by $\mathrm{d}\tau = -(\chi_l\phi_x + \chi_c)\mathrm{d}z/\mu$, with ϕ_x the normalized Voigt profile function, χ_c and χ_l the continuum and line opacities, and z the distance along the normal to the atmosphere. Hereafter, we omit the τ dependence of the intensity and source function for notational simplicity. The monochromatic source function is given by

$$S_x = \frac{\phi_x S_{lx} + rB}{\phi_x + r}, \tag{2}$$

where $r = \chi_c/\chi_l$, and B is the Planck function at the line frequency. The line source function is given by

$$S_{lx} = (1-\epsilon)\bar{J}_x + \epsilon B, \tag{3}$$

where ϵ is the collisional destruction probability. The PRD scattering integral or mean PRD intensity is given by

$$\bar{J}_x = \int g^k_{xx'} J_{x'} \mathrm{d}x', \tag{4}$$

with the mean intensity

$$J_x = \frac{1}{2}\int I_{x\mu}\mathrm{d}\mu\,. \tag{5}$$

In Equation (4), $g^k_{xx'} = R_{k,\mathrm{AA}}(x,x')/\phi_x$, where $R_{k,\mathrm{AA}}$ with k = I, II, and III are the AA redistribution functions of Hummer (1962). Their functional as well as the graphical form can be found in Hummer (1962), Mihalas (1978) and Heinzel (1981).

3. Iterative methods for unpolarized PRD radiative transfer

We write the formal solution of the radiative transfer equation (1) as

$$I_{x\mu} = \Lambda_{x\mu}[S_x] + T_{x\mu}\ , \tag{6}$$

where $T_{x\mu}$ gives the transmitted specific intensity due to the incident radiation at the boundary and $\Lambda_{x\mu}$ is a $N \times N$ operator whose elements depend on the optical distances between the grid points, with N being the number of spatial grid points.

A suitable formal solution method for the numerical solution of Equation (1) is the short-characteristics method (Kunasz & Auer 1988; Auer & Paletou 1994; Auer et al. 1994). This method is based on the assumption that the variation of the source function with the optical depth along the ray under consideration is a parabola between three consecutive grid points. Thus, if M represents an upwind point, O represents the point of interest and P the downwind point, then the intensity at point O is given by

$$\begin{aligned} I_{x\mu,O} = {} & I_{x\mu,M}\mathrm{e}^{-\Delta\tau_M} + \Psi_{x,M}(\mu)S_{x,M} \\ & + \Psi_{x,O}(\mu)S_{x,O} + \Psi_{x,P}(\mu)S_{x,P}, \end{aligned} \tag{7}$$

where $\Delta\tau_M$ is the optical distance on segment MO, $\Psi_{x,M,O,P}$ are functions of the optical distances between O and M and between O and P, and $S_{x,M,O,P}$ are source function values at the points M, O, and P, respectively. However, at the boundaries a linear interpolation for the source function along the points M and O is used for the rays going out of such boundaries.

Following Trujillo Bueno (2003) we write the mean PRD intensity at the spatial grid point 'i' as

$$\begin{aligned} \bar{J}_{x,i} \;=\; & \int g^k_{xx'}[\Lambda_{x',i1}S^a_{x',1} + \cdots + \Lambda_{x',ii-1}S^a_{x',i-1} \\ & + \Lambda_{x',ii}S^b_{x',i} + \Lambda_{x',ii+1}S^c_{x',i+1} + \cdots \\ & + \Lambda_{x',iN}S^c_{x',N}]\mathrm{d}x' + \bar{T}_{x,i}\,, \end{aligned} \tag{8}$$

where $\bar{T}_{x,i}$ is given by Equation (4) but with $J_{x'}$ replaced by $T_{x'}$ (which is given by Equation (5) with $I_{x'\mu}$ replaced by $T_{x'\mu}$). For each frequency x, $\Lambda_{x,ii'}$ is obtained by integrating $\Lambda_{x\mu}$ over all the directions μ of the incoming and outgoing radiation beams of the angular quadrature chosen for the numerical integration. Furthermore, a, b and c are simply symbols that will be useful to indicate weather we choose the 'old' or the 'new' values of the source function. In the following subsections we, first, briefly recall the Jacobi iterative method, and then present the GS and SOR iterative schemes.

3.1. Jacobi iterative scheme

Let us recall first the Jacobi iterative scheme presented in PA95. This scheme is obtained by choosing in Equation (8) $a = c =$ old, but $b =$ new, which gives:

$$\bar{J}_{x,i} = \bar{J}^{\rm old}_{x,i} + \int g^k_{xx'} \Lambda_{x',ii}\, p_{x'}\, \delta S_{lx',i}\, {\rm d}x' \,, \tag{9}$$

where we have used Equation (2). In the above equation $p_x = \phi_x/(\phi_x + r)$ and $\delta S_{lx,i} = S^{\rm new}_{lx,i} - S^{\rm old}_{lx,i}$. Using Equation (9) in Equation (3), we obtain the following expressions for the line source function corrections:

$$\begin{aligned} &\delta S_{lx,i} - (1-\epsilon) \int g^k_{xx'}\, \Lambda_{x',ii}\, p_{x'} \delta S_{lx',i}\, {\rm d}x' \\ &= (1-\epsilon)\bar{J}^{\rm old}_{x,i} + \epsilon B - S^{\rm old}_{lx,i} \,. \end{aligned} \tag{10}$$

Following PA95 we define a frequency dependent residual as

$$r_{x,i} = (1-\epsilon)\bar{J}^{\rm old}_{x,i} + \epsilon B - S^{\rm old}_{lx,i} \,. \tag{11}$$

Thus at each depth point we have to solve N_x linear equations, where N_x is the number of frequency points. The simplest (but numerically expensive) way to find the solution of the system of linear equations (10) is by matrix inversion as follows:

$$\delta \boldsymbol{S} = \mathbf{A}^{-1} \boldsymbol{r}, \tag{12}$$

where at each depth point i, $\boldsymbol{r}$ is a vector of length N_x, and the matrix $\mathbf{A}$ is of dimension $N_x \times N_x$, and its elements are given by

$$A_{mn} = \delta_{mn} - (1-\epsilon)\tilde{g}^k_{mn}\, \Lambda_{n,ii}\, p_n \,; \quad m, n = 1, \cdots, N_x \,. \tag{13}$$

Here δ_{mn} is the Kronecker's symbol, $\tilde{g}^k_{mn}$ are the redistribution weights, and the indices m and n refer respectively to the discretized values of x and x'. Note that for isothermal slabs

the matrix **A** can be computed only once and can be inverted and stored. This method was referred to as the Frequency-by-Frequency (FBF) method by PA95, which was developed by the authors for type II redistribution. It is easy to note that the same method can be easily applied to the type I and type III redistributions and a linear combination of type II and type III redistributions without any further effort.

The above FBF method involves the inversion of a matrix, which can be huge for realistic problems. For this reason, PA95 proposed a faster but equally robust method for the case of a type II redistribution function. In the following sub-section we briefly discuss this more efficient method, which is presented in more detail in PA95.

3.1.1. CRD-CS or Core-Wing method for type II redistribution

It is well known that $g^{\rm II}_{xx'}$ behaves like CRD in the line core and like coherent scattering in the wings (see Mihalas 1978). Taking advantage of this fact, to reduce the computational cost involved in the calculation of $\delta S_{lx,i}$, one can introduce a core-wing approximation to the true redistribution function $g^{\rm II}_{xx'}$, namely

$$g^{\rm II}_{xx'} \approx \begin{cases} \phi_{x'}, & \text{for } x, x' \le x_c, \\ \delta(x - x'), & \text{for } x' > x_c. \end{cases} \tag{14}$$

Here x_c is called the separation frequency that distinguishes between the line core and the wing. PA95 showed that $x_c = 3.5$ Doppler widths is a physically reasonable choice and, hence, we adopt the same in this paper.

Substituting Equation (14) in Equation (10), the equation for $\delta S_{lx,i}$ takes the simpler form

$$\delta S_{lx,i} = \frac{r_{x,i} + (1 - \alpha_x)\Delta T_i}{1 - \alpha_x(1 - \epsilon)p_x\Lambda_{x,ii}}, \tag{15}$$

where α_x are the splitting coefficients that allow for a smooth transition between the core and the wing. In the core $\alpha_x = 0$ and in the wing $\alpha_x = g^{\rm II}_{xx}$. The frequency independent core integral ΔT_i is given by

$$\Delta T_i = (1 - \epsilon) \int_{core} \phi_{x'} p_{x'} \Lambda_{x',ii}\, \delta S_{lx',i}\, {\rm d}x'. \tag{16}$$

To evaluate ΔT_i, we consider only the core frequencies (i.e., $\alpha_x = 0$) in Equation (15) and then apply the operator $(1 - \epsilon) \int_{core} \phi_{x'} p_{x'} \Lambda_{x',ii}[\,]{\rm d}x'$. The resulting scalar equation for ΔT_i can be easily solved to obtain ΔT_i (see PA95 for more details). From Equation (15) we see that the wing frequencies drop out for $x \le x_c$, and in the wings the term multiplying $(1-\alpha_x)$

appears only as a frequency independent quantity. Thus, it is possible to find all the $\delta S_{lx,i}$ values from a simple scalar equation, thereby completely avoiding the solution of a system of equations irrespective of the number of frequency grid points.

3.1.2. Extending the CRD-CS method to type I and III redistribution

The extension of the CRD-CS method to type III redistribution has been given in Fluri et al. (2003). To this end, the type III redistribution function is approximated by assuming CRD in the core and by setting it to zero in the wings. This is justified because the type III redistribution function does not show coherent peaks in the wings (see Mihalas 1978). However, we find that for the pure type III redistribution case we have to approximate $R_{\rm III,AA}$ by CRD throughout the frequency bandwidth to compute $\delta S_{lx,i}$. Setting it to zero in the wings leads to convergence problems. In the case of a linear combination of $R_{\rm II,AA}$ and $R_{\rm III,AA}$ (see § 4.4, Equation (29)), we find that as long as elastic collisions are small we can approximate $R_{\rm II,AA}$ by CRD-CS and $R_{\rm III,AA}$ by CRD in the line core and set it to zero in the wings. However, when elastic collisions are large we can approximate $R_{\rm II,AA}$ by CRD-CS, but $R_{\rm III,AA}$ should be approximated by CRD throughout the line profile, otherwise we have convergence problems.

For soling the type I redistribution problem we approximate $R_{\rm I,AA}$ by CRD in the core and set it to zero in the wings for the computation of the $\delta S_{lx,i}$ corrections. This is justified as $R_{\rm I,AA}$ is a pure Doppler redistribution function and does not show coherent peaks in the wings (see Mihalas 1978).

3.2. Gauss-Seidel and SOR iterative schemes

The radiative transfer methods based on GS and SOR iterations were developed by TF95 for the CRD case. In this section we extend such methods to solve unpolarized PRD problems.

The GS iterative scheme is obtained by choosing c = old and $a = b$ = new in Equation (8). This gives

$$\bar{J}_{x,i} = \bar{J}^{\rm old+new}_{x,i} + \int g^k_{xx'} \Lambda_{x',ii}\, \delta S_{x',i}\, {\rm d}x', \tag{17}$$

where $\delta S_{x,i} = p_x\, \delta S_{lx,i}$ and $\bar{J}^{\rm old+new}_{x,i}$ is the mean PRD intensity calculated using the 'new' values of the source function at grid points $1, 2, \cdots, i-1$ and the 'old' values at points

$i, i+1, \cdots, N$. The line source function corrections are now given by

$$\delta S_{lx,i} - (1-\epsilon) \int g^k_{xx'} \Lambda_{x',ii}\, p_{x'} \delta S_{lx',i}\, \mathrm{d}x' = (1-\epsilon) \bar{J}^{\mathrm{old+new}}_{x,i} + \epsilon B - S^{\mathrm{old}}_{lx,i} \; . \tag{18}$$

To compute $\delta S_{lx,i}$ we can apply either the FBF or the CRD-CS method discussed in § 3.1. The SOR iterative scheme is obtained by doing the corrections as follows:

$$\delta S^{\mathrm{SOR}}_{lx,i} = \omega \delta S^{\mathrm{GS}}_{lx,i} \; , \tag{19}$$

where ω is a parameter with an optimum value between 1 and 2 which can be found using the method discussed in § 2.4 of TF95. The Optimum value of ω is the one that leads to the highest rate of convergence. We find that the SOR method cannot be combined with the CRD-CS method for type II redistribution, while it works fine with the FBF method. The reason could be the way the wings are handled in the CRD-CS method.

3.2.1. The standard GS and SOR techniques

It is worth noting that the GS iterative scheme is twice faster compared to the Jacobi scheme. A factor two of additional improvement can be achieved by implementing the symmetric GS scheme (see TF95; Trujillo Bueno 2003). To explain the symmetric GS scheme, we first recall the GS scheme briefly, which is explained in greater detail in TF95.

Following TF95, we consider two distinct parts: a incoming and outgoing.

1. Incoming part ($\mu < 0$): One starts from the upper boundary ($i = 1$ with i being the depth index), and determines the intensity of the incoming rays ($\mu < 0$) at all depths using the short-characteristics formal solver. Thus, at the end of the incoming section, one has calculated the incoming contribution to the mean PRD intensity, $\bar{J}_{x,i}(\mu < 0)$, at all the depth points ($i = 1, \cdots N$).

2. Outgoing part ($\mu > 0$): One now starts from the lower boundary ($i = N$). Given that at this point the intensity is known, one can easily compute the total mean PRD intensity $\bar{J}_{x,N}$. We then use it to calculate $\delta S_{lx,N}$ and thereby the new source function $S^{\mathrm{new}}_{x,N}$ at the lower boundary. Now for the next depth point $i = N-1$, to calculate I_{N-1} using Equation (7) GS uses $S^{\mathrm{new}}_{x,N}$, $S^{\mathrm{old}}_{x,N-1}$ and $S^{\mathrm{old}}_{x,N-2}$. Then we compute the outgoing contribution to $\bar{J}_{x,N-1}(\mu > 0)$. However, note that the incoming contribution to $\bar{J}_{x,N-1}(\mu < 0)$ was calculated with the old

values of the source function, namely $S^{\rm old}_{x,N}$, $S^{\rm old}_{x,N-1}$ and $S^{\rm old}_{x,N-2}$. Therefore, to calculate the actual $\bar{J}^{\rm old+new}_{x,N-1}$ we add the following correction :

$$\Delta\bar{J}^{\rm in}_{x,N-1} = \int g^k_{xx'}\Delta J^{\rm in}_{x',N-1}{\rm d}x', \tag{20}$$

where

$$\Delta J^{\rm in}_{x,N-1} = \frac{1}{2}\delta S_{x,N}\int_{-1}^{0}\Psi_{x,N}(\mu<0){\rm d}\mu\,. \tag{21}$$

Here "in" stands for the incoming pass (see below). Once the actual $\bar{J}^{\rm old+new}_{x,N-1}$ is found one computes $\delta S_{lx,N-1}$ and the new source function $S^{\rm new}_{x,N-1}$. Because $S^{\rm new}_{x,N-1}$ is available now, before going to the next depth point the following correction should be added to the intensity $I_{x\mu>0}(N-1)$:

$$\Delta I^{\rm in}_{x\mu>0}(N-1) = \Psi_{x,N-1}(\mu>0)\delta S_{x,N-1}. \tag{22}$$

The above procedure is then repeated for subsequent depth points. Clearly, unlike the Jacobi iterative scheme, the GS iterative method requires specific ordering of loops in the formal solver. The outermost loop is over the directions (first the incoming and then the outgoing rays). The next loop is over the spatial points, followed by the loop over different $|\mu|$ points. The innermost loop is over the frequencies.

3.2.2. The Symmetric GS and SOR techniques

The symmetric GS iterative scheme discussed by Trujillo Bueno (2003) is obtained by introducing one more outer loop, which first does the GS iteration starting with the incoming ray (which we call incoming pass), and then the GS iteration starting with the outgoing ray (which we call outgoing pass). In the incoming pass all the GS steps are exactly the same as those described above. In the case of the outgoing pass, we again consider two parts to describe the symmetric GS case, namely the outgoing and the incoming parts. Let us clarify these parts :

3. Outgoing part of the outgoing pass ($\mu>0$) : We start from the lower boundary ($i=N$) and compute the outgoing contribution to the $\bar{J}_{x,i}(\mu>0)$ quantity at all depth points using the source function computed newly from the incoming pass.

4. Incoming part of the outgoing pass ($\mu<0$) : We now start from the upper boundary. At the upper boundary ($i=1$), we can compute the new source function $S^{\rm new}_{x,1}$, as the intensity is known. For the next depth point $i=2$, we compute the intensity using $S^{\rm new}_{x,1}$,

$S^{\rm old}_{x,2}$, and $S^{\rm old}_{x,3}$. Note that the so-called $S^{\rm old}_{x,i}$ for $i \geq 2$ are the new source functions obtained from the incoming pass (see above). Thus, we can now compute the incoming contribution to the $\bar{J}_{x,2}(\mu < 0)$. However, the outgoing contribution to $\bar{J}_{x,2}(\mu > 0)$ was calculated with the old values of the source function, namely, $S^{\rm old}_{x,1}$, $S^{\rm old}_{x,2}$, and $S^{\rm old}_{x,3}$. Therefore to calculate the actual $\bar{J}^{\rm old+new}_{x,2}$, one has to add the following correction

$$\Delta\bar{J}^{\rm out}_{x,2} = \int g^k_{xx'} \Delta J^{\rm out}_{x',2}\, {\rm d}x', \tag{23}$$

where

$$\Delta J^{\rm out}_{x,2} = \frac{1}{2}\delta S_{x,1} \int_0^{+1} \Psi_{x,1}(\mu > 0) {\rm d}\mu\,. \tag{24}$$

In the above equations "out" denote the outgoing pass. Once the actual $\bar{J}^{\rm old+new}_{x,2}$ is found we can now compute the new source function $S^{\rm new}_{x,2}$. Since $S^{\rm new}_{x,2}$ is available, before going to the next depth point the following correction should be added to the intensity $I_{x\mu<0}(2)$:

$$\Delta I^{\rm out}_{x\mu<0}(2) = \Psi_{x,2}(\mu < 0)\delta S_{x,2}. \tag{25}$$

The above procedure is then repeated for subsequent depth points.

This scheme together with the incoming pass (1 and 2) and outgoing pass (3 and 4) is nothing but the symmetric GS iterative scheme (hereafter SYM-GS). Thus, each call to the formal solver produces as an output two truly GS iterations. Clearly, the incoming pass has a convergence rate equivalent to that of a lower triangular approximate operator method and the outgoing pass has a convergence rate equivalent to that of an upper triangular approximate operator method (see TF95). This symmetric GS scheme can be extended to SOR also, which is then called Symmetric SOR (Trujillo Bueno 2003). The advantage of SSOR is that it is less sensitive to the choice of the optimum value of ω as compared to SOR (see Fig. 1 of Trujillo Bueno 2003). Furthermore, unlike SOR, the SSOR method can be combined with standard acceleration techniques like Ng (see Auer 1987, 1991) or orthomin's acceleration (Vinsome 1976; Klein et al. 1989; Auer 1991).

4. The true error of the numerical solutions

Following Auer et al. (1994) we define three quantities that characterize any iterative scheme, namely (1) the maximum relative change R_c, (2) the maximum relative convergence error C_e, and (3) the maximum relative true error T_e. For a given level of grid resolution g at the nth iterative stage these three quantities are defined as follows:

$$R_c(n,g) = \max_{\tau,x}\left[\frac{|S_{lx}(n,g) - S_{lx}(n-1,g)|}{S_{lx}(n,g)}\right], \tag{26}$$

$$C_e(n,g) = \max_{\tau,x} \left[\frac{|S_{lx}(n,g) - S_{lx}(\infty,g)|}{S_{lx}(\infty,g)} \right], \tag{27}$$

$$T_e(n,g) = \max_{\tau,x} \left[\frac{|S_{lx}(n,g) - S_{lx}(\infty,\infty)|}{S_{lx}(\infty,\infty)} \right]. \tag{28}$$

In the above equations $(n = \infty, g)$ indicates that one is dealing with the fully converged solution on a grid resolution level g, while $(n = \infty, g = \infty)$ indicates the true solution on a grid of infinite resolution. $T_e(\infty, g)$ is nothing but the truncation error corresponding to a grid of finite resolution level g, and thus it determines the accuracy of the converged solution in that grid.

In this paper we find the fully converged solution on a given grid resolution level g, by iterating until $R_c < 10^{-10}$. Beyond this value R_c does not decrease any further, but simply fluctuates around it. The true solution required to calculate the true error is found by using a grid which is twice finer compared to the grid on which we seek the true error.

Following TF95, in this paper we use the true error to determine the convergence properties of the iterative schemes. Here we show that the true error not only depends on the resolution of the spatial grid and the accuracy of the formal solver, but also on the choice of the redistribution function. In the following subsections we discuss the true error separately for the $R_{\rm I,II,III,AA}$ functions and for cases with a linear combination of $R_{\rm II,AA}$ and $R_{\rm III,AA}$.

4.1. Pure Doppler redistribution - type I redistribution

We recall that physically this case represents an atom with two sharp upper and lower levels. Thus, the line is infinitely sharp in the rest frame of the atom. In the laboratory frame it is broadened by the Doppler effect. This idealized case can hardly be applied to interpret any spectral lines, nevertheless it is an interesting academic case to study as it allows to examine the effects of pure Doppler redistribution by a Maxwellian velocity distribution.

Figure 1 shows the convergence properties of different iterative schemes discussed in the previous section, applied here to type I redistribution. For all computations presented in this paper we consider the case of a semi-infinite atmosphere with the lower boundary condition $I_{x\mu}(\tau = T) = B$, and upper boundary condition $I_{x\mu}(\tau = 0) = 0$. The depth grid is constructed using the relation $\tau = \exp(-Z)$, where $Z = z/H$ (with H the scale height), and Z the height in units of H. We choose a uniform spacing of ΔZ. For all the figures presented in this paper we have chosen $\Delta Z = 0.25$ (which corresponds to 9 points per decade). A Gaussian quadrature with 3 inclinations $[0 < \mu < 1]$, and an equally spaced frequency grid with 41 points and a spacing of 0.25 Doppler widths are used. Note

that a frequency bandwidth of $0 \leq x \leq 10$ is more than sufficient, as we are considering a pure Doppler redistribution (with zero damping). The collisional destruction probability $\epsilon = 10^{-4}$. The Plank function B is set to unity. Unless stated otherwise we set the continuum parameter r to zero. From the left panel of Fig. 1 we see that the convergence behavior of the different iterative schemes are exactly the same as that discussed in TF95. We note that for type I redistribution we obtain a true error of 2.7×10^{-3}, while for the corresponding coherent scattering and CRD (with damping parameter $a = 0$) cases we get a true error of 3.5×10^{-3}, and 4.3×10^{-3}, respectively.

4.2. Doppler, Natural and Collisional Broadening - type III redistribution

Physically this case represents a resonance line with its upper level both radiatively and collisionally broadened. Collisions are so frequent that there is CRD in the rest frame of the atom.

Figure 2 shows the convergence properties of the different iterative schemes, applied here to type III redistribution. Model parameters are the same as those for type I redistribution, but now the damping parameter $a = 10^{-3}$. The angular and depth grids used for the computation are exactly the same as those used for type I redistribution. However, a non-uniform frequency grid that extends up to 1000 Doppler widths from the line center is used (as now $a \neq 0$). We note that for type III redistribution we obtain $T_e = 2.3 \times 10^{-3}$, which is nearly the same true error as that obtained for the corresponding CRD case (with $a = 10^{-3}$). This is expected, as it is well known that $R_{\rm III,AA}$, in the rest frame of the atom behaves like CRD.

4.3. Doppler and Natural Broadening - type II redistribution

Physically type II redistribution represents the case of a line with an infinitely sharp lower level and an upper level broadened by radiative decay only. In the rest frame of the atom the absorption profile is a Lorentzian and the scattering is completely coherent. This type of scattering problem is essential to model strong resonance lines, formed in low density media.

Figure 3 shows the convergence properties of different iterative schemes, applied here to the type II redistribution problem. The model parameters and the various grids used for the computation are the same as those used in § 4.2 for type III redistribution. We point out

that the SSOR method works well when combined with the FBF technique, while it doesn't work properly when combined with the CRD-CS method. The reason is probably due to the way the wings are handled in the CRD-CS method. For type II redistribution we obtain $T_e = 0.12$, which is pretty a high value compared to that obtained in the type I, III and CRD cases. It is well known that one needs a much more refined frequency grid for $R_{\rm II,AA}$ than for the other redistribution functions because the asymptotic large scale behavior of the transfer equation for $R_{\rm II,AA}$ is like a space and frequency diffusion equation (see Frisch 1988). However, we checked that use of a frequency grid even finer than the non-uniform frequency grid mentioned above does not change the T_e value quoted above. Such a high value of T_e could be due to the fact that $R_{\rm II,AA}$ has coherent peaks in the wings, while other functions do not have coherent peaks. Furthermore, in the case of $R_{\rm II,AA}$ the wings cannot be easily thermalized (see Frisch 1980). It is worth to note that very far in the wings only diffusion in space remains. Such a regime is encountered only in pure $R_{\rm II,AA}$ problems. The presence of a background continuum or of some elastic collisions will hide this very far wing regime and thereby decreases T_e (see below).

We made a detailed study of the true error for the $R_{\rm II,AA}$ redistribution function case using the SYM-GS iterative method. Figure 4, shows the true error for different ϵ values. Note that the true error decreases when the non-LTE parameter ϵ increases (i.e., when the number of scattering events decreases). In Table 1 we present the true error for different resolutions of the depth grid. As expected, the true error decreases as the grid resolution increases.

Figure 5 shows the behavior of the true error for type II redistribution when a background continuum is included. Clearly, the addition of the continuum decreases the true error substantially, as the wings can then be thermalized. Note that even with an opacity ratio r as small as 10^{-12} the true error decreases to nearly 3.5×10^{-3}, from $T_e = 0.12$ for the pure line case. Since in practical problems a background continuum is always present, we can conclude that the true error of the numerical methods based on operator splitting for type II redistribution can be made significantly small. For example, it is 0.2 % when $r = 10^{-4}$ and $\Delta Z = 0.25$.

4.4. Linear combination of $R_{\rm II,AA}$ and $R_{\rm III,AA}$

We now consider a more realistic case characterized by the following weighted combination of type II and type III redistribution (e.g., Stenflo 1994) :

$$R_{\rm AA}(x, x') = \gamma R_{\rm II,AA}(x, x') + (1 - \gamma) R_{\rm III,AA}(x, x'), \tag{29}$$

where $\gamma = 1/(1 + \Gamma_{\rm E}/\Gamma_{\rm R})$, with $\Gamma_{\rm E}$ the elastic collisional rate and $\Gamma_{\rm R}$ the radiative rate.

Figure 6 shows the behavior of the true error for different choices of the elastic collision parameter $\Gamma_{\rm E}/\Gamma_{\rm R}$. The true error corresponding to $\Gamma_{\rm E}/\Gamma_{\rm R} = 0$ is nothing but that corresponding to the pure $R_{\rm II,AA}$ case, which shows the largest value for the truncation error. Introducing a small mix of type III redistribution through the contribution of elastic collisions results in a decrease of the true error. Already for $\Gamma_{\rm E}/\Gamma_{\rm R} = 0.1$, the true error is nearly the same as that corresponding to the CRD case. This again shows that the coherent peaks of $R_{\rm II,AA}$ are responsible for a large truncation error in the case of pure type II redistribution without any background continuum.

5. Polarized PRD radiative transfer equation

In this paper we restrict ourselves to situations where the radiation field is axially symmetric. This condition is satisfied only for one-dimensional plane-parallel or spherical atmospheres with either no magnetic field, or a micro-turbulent and isotropic field, or a micro-structured magnetic field with a fixed inclination and a random azimuth. Here we consider the case of a plane-parallel atmosphere with zero magnetic field.[1] An axially symmetric polarized radiation field is described by the Stokes parameters I and Q (see Chandrasekhar 1950), where I denotes the intensity and Q the linear polarization (i.e., the difference between the intensity components parallel and perpendicular to a given reference direction in the plane perpendicular to the direction of the ray under consideration). In this paper, the positive Q direction is defined in the plane containing the direction of the ray and the vertical Z-axis. The one-dimensional transfer equation for the Stokes vector components $I_{x\mu,j} = (I, Q)$ for $j = 0, 1$ is given by

$$\frac{\mathrm{d}}{\mathrm{d}\tau} I_{x\mu,j}(\tau) = I_{x\mu,j}(\tau) - S_{x\mu,j}(\tau). \tag{30}$$

The source vector components $S_{x\mu,j} = (S^I_{x\mu}, S^Q_{x\mu})$ for $j = 0, 1$ are of the form

$$S_{x\mu,j} = \frac{\phi_x S_{lx\mu,j} + r B U_j}{\phi_x + r}, \tag{31}$$

[1] We remark that a microturbulent magnetic field can be taken into account by simply replacing $W_2(J_l, J_u)$ (see § 5.1. for its definition) by $H_2\, W_2(J_l, J_u)$, where H_2 is the so-called Hanle depolarization factor. H_2 is unity when the magnetic strength is zero. The explicit form of H_2 for an isotropic magnetic field and a horizontal magnetic field with random azimuth can be found in Stenflo (1994) and Landi Degl'Innocenti & Landolfi (2004).

where $U_j = (1, 0)$ for $j = 0, 1$, and the line source vector components $S_{lx\mu,j}$ are given by (e.g., Rees & Saliba 1982)

$$S_{lx\mu,j} = \epsilon B U_j + \int_{-\infty}^{+\infty} \mathrm{d}x' \frac{1}{2} \int_{-1}^{+1} \mathrm{d}\mu' \times \sum_{j'=0}^{1} \left[\mathbf{R}(x, x'; \mu, \mu')\right]_{jj'} I_{x'\mu',j'}. \quad (32)$$

In the above equation $\left[\mathbf{R}(x, x'; \mu, \mu')\right]_{jj'}$ are the elements of the scattering redistribution matrix $\mathbf{R}(x, x'; \mu, \mu')$ for the non-magnetic case (Rees & Saliba 1982; Domke & Hubeny 1988). In the following subsections we first discuss the redistribution matrix for the non-magnetic case, and then present the decomposition technique proposed by Frisch (2007). This is because the iterative algorithms given in this paper are based on the ensuing equations deduced in § 5.2.

5.1. Redistribution matrix

A hybrid approximation to $\mathbf{R}(x, x'; \mu, \mu')$ was introduced by Rees & Saliba (1982) :

$$\mathbf{R}(x, x'; \mu, \mu') = (1 - \epsilon) g^k_{xx'} \mathbf{P}(\mu, \mu'), \quad (33)$$

where the phase matrix $\mathbf{P}(\mu, \mu')$ is given by (e.g., Landi Degl'Innocenti & Landolfi 2004; Bommier 1997)

$$\mathbf{P}(\mu, \mu') = \sum_{K=0,2} W_K(J_l, J_u) \mathbf{P}^K_{\mathrm{R}}(\mu, \mu'). \quad (34)$$

The coefficient $W_0(J_l, J_u) = 1$, with J_l and J_u being the total angular momentum quantum numbers of the lower and upper levels, respectively. The coefficient $W_2(J_l, J_u)$ characterizes the maximum linear polarization that can be produced in the line. In the case of a normal Zeeman triplet ($J_l = 0, J_u = 1$), $W_2(J_l, J_u) = 1$, and $\mathbf{P}(\mu, \mu') = \mathbf{P}_{\mathrm{R}}(\mu, \mu')$ is the so-called Rayleigh phase matrix. Even though the figures of this paper correspond to the case of a normal Zeeman triplet, we present the equations for the more general case of arbitrary values of $W_K(J_l, J_u)$. The Rayleigh phase matrix multipolar components $\mathbf{P}^K_{\mathrm{R}}(\mu, \mu')$ are given by (see Landi Degl'Innocenti 1984, written here for the azimuthally symmetric case)

$$\left[\mathbf{P}^K_{\mathrm{R}}(\mu, \mu')\right]_{jj'} = \tilde{\mathcal{T}}^K_0(j, \theta) \tilde{\mathcal{T}}^K_0(j', \theta'), \quad (35)$$

where $j, j' = 0, 1$. The notation $\tilde{\mathcal{T}}^K_Q(j, \theta)$ was introduced by Frisch (2007, see her Equation (28)), where for each K, Q takes values between $-K$ to $+K$ in steps of unity. These

quantities are related to the irreducible tensors for polarimetry $\mathcal{T}^K_Q(j,\mathbf{\Omega})$ introduced by Landi Degl'Innocenti (1984), where $\mathbf{\Omega} = (\theta,\chi)$ denote the ray direction (see Frisch 2007). Since here we are dealing with the azimuthally symmetric case, the relevant quantities corresponding to $Q = 0$ are (see Table 5.6 of Landi Degl'Innocenti & Landolfi 2004)

$$\tilde{\mathcal{T}}^0_0(0,\theta) = 1\,; \quad \tilde{\mathcal{T}}^2_0(0,\theta) = \frac{1}{2\sqrt{2}}(3\mu^2-1),$$
$$\tilde{\mathcal{T}}^0_0(1,\theta) = 0\,; \quad \tilde{\mathcal{T}}^2_0(1,\theta) = -\frac{3}{2\sqrt{2}}(1-\mu^2). \tag{36}$$

In Equation (33), $\epsilon = \Gamma_{\rm I}/(\Gamma_{\rm I}+\Gamma_{\rm R})$ with $\Gamma_{\rm I}$ being the inelastic collisional rate and $\Gamma_{\rm R}$ the radiative rate. However, Equation (33) is only an approximate form of the redistribution matrix as it does not take into account the effect of elastic ($\Gamma_{\rm E}$) and depolarizing ($D^{(K)}$) collisional rates. The first quantum mechanical calculation of the redistribution matrix for the resonance polarization, taking into account the effect of elastic collisions was performed by Omont et al. (1972). Starting from the work of Omont et al. (1972), Domke & Hubeny (1988) derived a tractable analytic expression of the redistribution matrix. It is worth to note that the redistribution matrix that was derived by Domke & Hubeny (1988), is very general, namely, it depends on the angle-dependent redistribution functions of Hummer (1962). However for computational simplicity, following Rees & Saliba (1982), Nagendra (1994, see also Faurobert-Scholl 1992) used the angle-averaged version of the Domke-Hubeny (DH) redistribution matrix. Following Bommier (1997) we write this redistribution matrix as follows:

$$\mathbf{R}_{\rm DH}(x,x';\mu,\mu') = \textstyle\sum_{K=0,2} W_K(J_l,J_u)$$
$$\times \left\{\alpha\, g^{\rm II}_{xx'} + [\beta^{(K)}-\alpha]\, g^{\rm III}_{xx'}\right\} \mathbf{P}^K_{\rm R}(\mu,\mu'), \tag{37}$$

where the branching ratios α and $\beta^{(K)}$ are given by

$$\alpha = \frac{\Gamma_{\rm R}}{\Gamma_{\rm R}+\Gamma_{\rm I}+\Gamma_{\rm E}}, \tag{38}$$

$$\beta^{(K)} = \frac{\Gamma_{\rm R}}{\Gamma_{\rm R}+\Gamma_{\rm I}+D^{(K)}}. \tag{39}$$

Note that $D^{(0)} = 0$, and also that the factor $(1-\epsilon)$ is contained in the branching ratios.

It is worth to clarify certain important points related to these branching ratios (see also Nagendra 1994). In astrophysics one expects that the branching ratios add up to unity. However, from Equation (37) we see that the branching ratios add up to give $\left[\alpha+\beta^{(K)}-\alpha\right] = \beta^{(K)}$, which for $K = 0$ is nothing but $(1-\epsilon)$ and for $K = 2$ is $(1-\epsilon)/\left[1+\delta^{(2)}(1-\epsilon)\right]$ with $\delta^{(2)} = D^{(2)}/\Gamma_{\rm R}$. We note that these are indeed the factors that appear in the line source

function expressions for Stokes I and Stokes Q (namely S_0^0 and S_0^2 or ρ_0^0 and ρ_0^2) in the CRD case formulated (see Trujillo Bueno & Manso Sainz 1999; Landi Degl'Innocenti & Landolfi 2004). It is important to note that some authors (e.g., Faurobert-Scholl 1992; Nagendra 1994), write the factor $(1-\epsilon)$ before the second term of Equation (32) and renormalize the branching ratios α and $\beta^{(K)}$ by $(1-\epsilon)$, namely

$$
\begin{aligned}
(\alpha)^{\rm old} &= \frac{\alpha}{1-\epsilon} = \frac{\Gamma_{\rm R}+\Gamma_{\rm I}}{\Gamma_{\rm R}+\Gamma_{\rm I}+\Gamma_{\rm E}}, \\
\left[\beta^{(K)}\right]^{\rm old} &= \frac{\beta^{(K)}}{1-\epsilon} = \frac{\Gamma_{\rm R}+\Gamma_{\rm I}}{\Gamma_{\rm R}+\Gamma_{\rm I}+D^{(K)}}.
\end{aligned}
\tag{40}
$$

The approximate form of $\mathbf{R}(x,x';\mu,\mu')$ given in Equation (33) was used in plane-parallel polarized radiative transfer by Rees & Saliba (1982) and Faurobert (1987, 1988), with $g^{\rm II}_{xx'}$. These authors used Feautrier's (1964) method to solve the polarized transfer equation. A discrete space method was used by Nagendra (1986, 1988, 1989) for the same problem but in spherical atmospheres. McKenna (1984) used an integral equation approach to solve the same problem with a linear combination of $g^{\rm II}_{xx'}$ and $g^{\rm III}_{xx'}$ (see Equation (29)). The DH redistribution matrix given in Equation (37) was used in plane-parallel polarized radiative transfer computations by Faurobert-Scholl (1992, 1993). The same problem was solved by Nagendra (1994, 1995) but in spherical atmospheres. As already mentioned in the introduction such methods are computationally expensive.

A Jacobi based ALI method to solve the polarized radiative transfer equation with the hybrid approximation for the redistribution matrix and $g^{\rm II}_{xx'}$ was developed by Paletou & Faurobert-Scholl (1997). They extended the CRD-CS method of PA95 to scattering polarization. Trujillo Bueno & Manso Sa (1999) generalized the symmetric GS and SOR methods of TF95 to CRD polarized radiative transfer, with the relevant equations formulated within the framework of the quantum theory of spectral line polarization described in the monograph by Landi Degl'Innocenti & Landolfi (2004). In this paper we generalize these symmetric GS and SOR methods to solve the above-mentioned PRD problem. We consider both, the hybrid approximation and the DH redistribution matrix. In the next section we present the Jacobi, GS and SOR iterative methods to solve polarized radiative transfer problems with the DH redistribution matrix.

5.2. Decomposition in the irreducible basis

From Equations (31) and (32) we see that unlike the unpolarized case, the line source vector components now depend not only on the frequency x but also on the orientation μ of the radiation beams. In the case of CRD the line source vector components depend only

on μ and are independent of x. To reduce the computational cost, Faurobert-Scholl et al. (1997, see also Paletou & Faurobert-Scholl 1997) used a factorized form of $\mathbf{P}(\mu, \mu')$ given by Ivanov (1995), which allowed them to transform or reduce the polarized CRD transfer equation to a 2×2 basis wherein the source vector components are independent of μ. To this 2×2 matrix transfer equation they applied a Jacobi iterative scheme to solve the problem.

The factorization of the Rayleigh phase matrix into a product of two 2×2 matrices that depend separately on μ and μ' is not unique (see Frisch 2007). Such a factorization comes out naturally if one uses the $\mathcal{T}^K_Q(j, \mathbf{\Omega})$ irreducible tensors (see Landi Degl'Innocenti 1984) to derive the Rayleigh phase matrix (see Equation (35)). Using the irreducible tensors $\mathcal{T}^K_Q(j, \mathbf{\Omega})$, Frisch (2007) provided a simple way of transforming or reducing the Stokes vector components to irreducible tensors in the case of the Hanle effect regime. Such a transformation is referred to as the "decomposition" of the Stokes vector components. We note that such a decomposition comes out naturally in the density matrix theory of spectral line polarization (see Landi Degl'Innocenti & Landolfi 2004). Furthermore, it is well known that the density matrix and the scattering formalisms (that we adopt in this paper) are equivalent for a two-level atom without lower-level polarization and stimulated emission. However, in this paper we use the decomposition technique proposed by Frisch (2007), but applied here to the axially symmetric case. For clarity, we present some important steps of this decomposition. For more details the reader is referred to Frisch (2007).

For the azimuthally symmetric case the Stokes vector component decomposition given by Frisch (2007) takes the following form (in the notations used in this paper) :

$$I_{x\mu,j} = \sum_{K=0,2} \tilde{\mathcal{T}}^K_0(j, \theta)\, (I_{x\mu})^K_0, \tag{41}$$

with similar equations relating U_j, $S_{x\mu,j}$ and $S_{lx\mu,j}$ to U^K_0, $(S_x)^K_0$ and $(S_{lx})^K_0$, respectively. Note that $U^0_0 = 1$ and $U^2_0 = 0$. The quantities $(I_{x\mu})^K_0$ and $(S_x)^K_0$ are called the irreducible tensor components of the Stokes and the source vector components, respectively.

Substituting Equations (35), (37) and (41) in Equations (30)–(32), it can be shown that $(I_{x\mu})^K_0$ satisfies a transfer equation similar to Equation (30) but with $I_{x\mu,j}$ and $S_{x\mu,j}$ replaced by $(I_{x\mu})^K_0$ and $(S_{x\mu})^K_0$, respectively. Furthermore, $(S_{x\mu})^K_0$ is given by Equation (31) but with $S_{lx\mu,j}$ and U_j replaced by $(S_{x\mu})^K_0$ and U^K_0, respectively. The irreducible components of the line source vector are now given by

$$(S_{lx})^K_0 = \epsilon B U^K_0 + W_K(J_l, J_u)(\bar{J}_x)^K_0, \tag{42}$$

where

$$(\bar{J}_x)^K_0 \;=\; \int_{-\infty}^{+\infty} \mathrm{d}x'$$

$$\times \left\{ \alpha g^{\rm II}_{xx'} + \left[\beta^{(K)} - \alpha \right] g^{\rm III}_{xx'} \right\} (J_{x'})^K_0. \tag{43}$$

In the above equation the angle integrated irreducible tensor is given by

$$(J_{x'})^K_0 = \sum_{K'=0,2} \frac{1}{2} \int_{-1}^{+1} \Psi^{KK'}_0(\mu') (I_{x'\mu'})^{K'}_0(\tau) {\rm d}\mu', \tag{44}$$

where

$$\Psi^{KK'}_0(\mu') = \sum_{j'=0}^{1} \tilde{\mathcal{T}}^K_0(j', \theta') \tilde{\mathcal{T}}^{K'}_0(j', \theta'). \tag{45}$$

Clearly, the advantage of this decomposition is that the irreducible tensor components of the source vectors are now independent of the orientation μ of the radiation beam.

Following Frisch (2007) we now introduce the 2-component Stokes and source vectors in the irreducible basis

$$\boldsymbol{\mathcal{I}}_{x\mu} = \left[(I_{x\mu})^0_0,\, (I_{x\mu})^2_0 \right]^{\rm T}; \quad \boldsymbol{\mathcal{S}}_x = \left[(S_x)^0_0,\, (S_x)^2_0 \right]^{\rm T}. \tag{46}$$

In the above vector notation, the transfer equation in the irreducible basis can be written as

$$\frac{\rm d}{{\rm d}\tau} \boldsymbol{\mathcal{I}}_{x\mu}(\tau) = \boldsymbol{\mathcal{I}}_{x\mu}(\tau) - \boldsymbol{\mathcal{S}}_x(\tau), \tag{47}$$

where $\boldsymbol{\mathcal{S}}_x$ is given by Equation (31), but with $S_{lx\mu,j}$ and U_j replaced by $\boldsymbol{\mathcal{S}}_{lx}$ and $\boldsymbol{\mathcal{U}}$, respectively. Here $\boldsymbol{\mathcal{U}} = (1, 0)^{\rm T}$, and

$$\boldsymbol{\mathcal{S}}_{lx} = \epsilon B \boldsymbol{\mathcal{U}} + \mathbf{W}\, \overline{\boldsymbol{\mathcal{J}}}_x. \tag{48}$$

In the above equation

$$\overline{\boldsymbol{\mathcal{J}}}_x = \int_{-\infty}^{+\infty} \mathbf{N}_{xx'} \boldsymbol{\mathcal{J}}_{x'}\, {\rm d}x', \tag{49}$$

where

$$\mathbf{N}_{xx'} = g^{\rm II}_{xx'} \alpha \mathbf{E} + g^{\rm III}_{xx'} \left(\mathcal{B} - \alpha \mathbf{E} \right), \tag{50}$$

and the 2-component mean intensity vector

$$\boldsymbol{\mathcal{J}}_{x'} = \frac{1}{2} \int_{-1}^{+1} \boldsymbol{\Psi}(\mu')\, \boldsymbol{\mathcal{I}}_{x'\mu'}\, {\rm d}\mu'. \tag{51}$$

In Equations (50) and (51), $\mathbf{E}$ is a 2×2 identity matrix, while $\mathbf{W} = {\rm diag}[W_0, W_2]$ and $\boldsymbol{\mathcal{B}} = {\rm diag}[\beta^{(0)}, \beta^{(2)}]$ are 2×2 matrices. Note that since the matrix $\boldsymbol{\mathcal{B}}$ is diagonal, the matrix $\mathbf{N}_{xx'}$ is also diagonal. The explicit form of the 2×2 matrix $\boldsymbol{\Psi}$ formed by the elements $\Psi^{KK'}_0$ can be found in Appendix A of Frisch (2007). In the next section we apply the Jacobi, GS and SOR iterative schemes to Equations (47)–(51).

6. Iterative methods for polarized PRD radiative transfer

The formal solution of Equation (47) is given by Equation (6), but with $I_{x\mu}$, $\Lambda_{x\mu}$, S_x and $T_{x\mu}$ replaced by $\boldsymbol{\mathcal{I}}_{x\mu}$, $\boldsymbol{\Lambda}_{x\mu}$, $\boldsymbol{\mathcal{S}}_x$, and $\boldsymbol{T}_{x\mu}$, respectively. Here $\boldsymbol{T}_{x\mu}$ is the transmitted 2-component Stokes vector due to the incident radiation at the boundaries, and $\boldsymbol{\Lambda}_{x\mu}$ is a $2N \times 2N$ operator. For given depth indices i, i', $\boldsymbol{\Lambda}_{x\mu,ii'}$ is a 2×2 block. We use again the short-characteristics method as the formal solver, but now applied to the vector transfer equation (47).

As in Equation (8), we now write the 2-component mean intensity vector as

$$\begin{aligned} \boldsymbol{\mathcal{J}}_{x,i} &= \boldsymbol{\Lambda}_{x,i1}\boldsymbol{\mathcal{S}}^a_{x,1} + \cdots + \boldsymbol{\Lambda}_{x,ii-1}\boldsymbol{\mathcal{S}}^a_{x,i-1} \\ &\quad + \boldsymbol{\Lambda}_{x,ii}\boldsymbol{\mathcal{S}}^b_{x,i} + \boldsymbol{\Lambda}_{x,ii+1}\boldsymbol{\mathcal{S}}^c_{x,i+1} + \cdots \\ &\quad + \boldsymbol{\Lambda}_{x,iN}\boldsymbol{\mathcal{S}}^c_{x,N} + \boldsymbol{T}_{x,i}\ , \end{aligned} \tag{52}$$

where $\boldsymbol{T}_{x,i}$ is given by Equation (51) but with $\boldsymbol{\mathcal{I}}_{x\mu}$ replaced by $\boldsymbol{T}_{x\mu}$. The 2×2 matrix $\boldsymbol{\Lambda}_{x,ii'}$ is given by

$$\boldsymbol{\Lambda}_{x,ii'} = \frac{1}{2}\int_{-1}^{+1} \boldsymbol{\Psi}(\mu)\, \boldsymbol{\Lambda}_{x\mu,ii'}\, \mathrm{d}\mu. \tag{53}$$

Note that unlike the unpolarized case (see Equation (8)), at each depth we now have to perform a matrix operation involving a 2×2 matrix and a 2 column vector. In the following subsections we successively present the Jacobi, GS and SOR iterative schemes.

6.1. Jacobi Iterative scheme

It is straightforward to generalize the Jacobi scheme discussed in § 3.1 to the scattering polarization case. With this iterative scheme, the equations for the 2-component line source vector corrections are given by

$$\delta\boldsymbol{\mathcal{S}}_{lx,i} - \mathbf{W}\int_{-\infty}^{+\infty} \mathbf{N}_{xx'} p_{x'} \boldsymbol{\Lambda}_{x',ii}\, \delta\boldsymbol{\mathcal{S}}_{lx',i}\, \mathrm{d}x' = \boldsymbol{\mathcal{R}}_{x,i}\,, \tag{54}$$

where

$$\boldsymbol{\mathcal{R}}_{x,i} = \epsilon\, B\boldsymbol{\mathcal{U}} + \mathbf{W}\, \overline{\boldsymbol{\mathcal{J}}}^{\,\mathrm{old}}_{x,i} - \boldsymbol{\mathcal{S}}^{\mathrm{old}}_{lx,i}\,. \tag{55}$$

As discussed in § 3.1. the system of linear equation (54) can be solved by the FBF method, namely

$$\boldsymbol{\mathcal{A}}\,\delta\boldsymbol{\mathcal{S}} = \boldsymbol{\mathcal{R}}, \tag{56}$$

where at each depth point i, $\boldsymbol{\mathcal{R}}$ is a vector of length $2N_x$, and the matrix $\boldsymbol{\mathcal{A}}$ is of dimension $2N_x \times 2N_x$. For a given depth point i, and given frequencies x, x', $\boldsymbol{\mathcal{A}}$ is a 2×2 block denoted by $\boldsymbol{\mathcal{A}}^2$, and given by the expression

$$\boldsymbol{\mathcal{A}}^2 = \delta_{mn}\,\mathbf{E} - \mathbf{W}\,\mathbf{N}_{mn}\,p_n\,\boldsymbol{\Lambda}_{n,ii}\,; \quad m, n = 1, \cdots, N_x. \tag{57}$$

Clearly, the above FBF method is numerically much more expensive compared to the unpolarized case, as the size of the matrix $\boldsymbol{\mathcal{A}}$ is now twice larger. The FBF method was actually generalized by Sampoorna et al. (2008) for the weak field regime of the Hanle effect (with PRD). This method has also been used by Frisch et al. (2009) for the Hanle effect of a turbulent magnetic fields with a finite correlation length (and with CRD).

As already discussed in § 3.1. for the unpolarized case, the CRD-CS method is computationally less expensive, but is as robust as the FBF method. This CRD-CS method was extended to scattering polarization (non-magnetic) by Paletou & Faurobert-Scholl (1997) for the hybrid approximation that uses $g^{\rm II}_{xx'}$. This method was later extended to the Hanle effect case by Fluri et al. (2003). They used the weak field Hanle redistribution matrix of Bommier (1997), the so-called approximation-III, which reduces to the DH redistribution matrix for the zero magnetic field case. In the following subsection we briefly recall the CRD-CS method of Fluri et al. (2003), applied here to non-magnetic case. The main difference with the equations presented in this paper is that we use the decomposition technique of Frisch (2007), while Fluri et al. (2003) use the traditional Fourier-azimuthal expansion technique discussed in Nagendra et al. (1998).

6.1.1. CRD-CS or core-wing method for the DH redistribution matrix

As discussed in § 3.1.1 and 3.1.2, in Equation (54) we approximate $g^{\rm II}_{xx'}$ by Equation (14) and $g^{\rm III}_{xx'}$ by $\phi_{x'}$ in the line core ($x \le x_c$), but set it to zero in the wings ($x > x_c$). This gives (using Equation (50))

$$\delta\boldsymbol{\mathcal{S}}_{lx,i} = \frac{\boldsymbol{\mathcal{R}}_{x,i} + (1-\alpha_x)\,\mathbf{W}\,\boldsymbol{\mathcal{B}}\,\Delta\boldsymbol{\mathcal{T}}_i}{1 - \alpha_x\,\alpha\,p_x\,\mathbf{W}\,\boldsymbol{\Lambda}_{x,ii}}\,. \tag{58}$$

Following Fluri et al. (2003, see also Paletou & Faurobert-Scholl 1997; Nagendra et al. 1999), one can show that

$$\Delta\boldsymbol{\mathcal{T}}_i = \left[\mathbf{E} - \int_{-\infty}^{+\infty} \mathrm{d}x\,\phi_x\,p_x\,\boldsymbol{\Lambda}_{x,ii}\,\cdot\,\mathbf{W}\,\boldsymbol{\mathcal{B}}\right]^{-1}\,\bar{\boldsymbol{\mathcal{R}}}_i, \tag{59}$$

where

$$\bar{\boldsymbol{\mathcal{R}}}_i = \int_{-x_c}^{+x_c} \phi_x\,p_x\,\boldsymbol{\Lambda}_{x,ii}\,\boldsymbol{\mathcal{R}}_{x,i}\,\mathrm{d}x. \tag{60}$$

Note from Equation (58) that in the core (when $\alpha_x = 0$) the denominator reduces to unity (i.e., we are left with a simple summation), while in the wings the term multiplying $(1 - \alpha_x)$ appears as a frequency independent quantity.

6.2. GS and SOR iterative schemes

These radiative transfer methods were developed by Trujillo Bueno & Manso Sainz (1999) for the non-magnetic and micro-turbulent field CRD cases and by Manso Sainz & Trujillo Bueno (1999) for the CRD case of a deterministic magnetic field in the Hanle effect regime. Here we present the generalization of these methods to the PRD problem of resonance line polarization in the absence or in the presence of a weak magnetic field which does not break the axial symmetry of the problem (e.g., a microturbulent field).

The GS iterative scheme is obtained by choosing c = old and $a = b$ = new in Equation (52), which gives

$$\boldsymbol{\mathcal{J}}_{x,i} = \boldsymbol{\mathcal{J}}_{x,i}^{\rm old+new} + \boldsymbol{\Lambda}_{x,ii}\,\delta\boldsymbol{\mathcal{S}}_{x,i}\,, \tag{61}$$

where $\boldsymbol{\mathcal{J}}_{x,i}^{\rm old+new}$ is the 2-component mean intensity vector calculated using 'new' values of the source vector $\boldsymbol{\mathcal{S}}_{x,i}$ at grid points $1, 2, \cdots, i-1$, and the 'old' values at $i, i+1, \cdots, N$. The line source vector corrections are given by Equation (54), but with

$$\boldsymbol{\mathcal{R}}_{x,i} = \epsilon\, B\,\boldsymbol{\mathcal{U}} + \mathbf{W}\,\overline{\boldsymbol{\mathcal{J}}}_{x,i}^{\rm old+new} - \boldsymbol{\mathcal{S}}_{lx,i}^{\rm old}\,. \tag{62}$$

The line source vector corrections can be computed using either the FBF or the CRD-CS methods discussed in § 6.1. Note that the GS as well as the SYM-GS iterative algorithms discussed in § 3.2 can be extended straightforwardly to the polarized case. The only difference is that we are now dealing with a 2-component source vector, with intensity as well as mean intensity vectors, and with an approximate lambda operator which is now a 2×2 block for any given depth and frequency. For example, in the several correction terms that one needs to consider in a SYM-GS algorithm, namely Equations (20)–(25), we have to replace simply the unpolarized quantities $J_{x,i}$, $\bar{J}_{x,i}$ and $S_{x,i}$ by the polarized 2-component vectors $\boldsymbol{\mathcal{J}}_{x,i}$, $\overline{\boldsymbol{\mathcal{J}}}_{x,i}$ and $\boldsymbol{\mathcal{S}}_{x,i}$, respectively, to be able to apply those equations to the polarized case. Therefore, unlike in the unpolarized case we now have to do several matrix manipulations (see, e.g., Equations (56) and (58)).

The SOR iterative scheme is obtained by doing the corrections as follows:

$$\delta\boldsymbol{\mathcal{S}}_{lx,i}^{\rm SOR} = \omega\,\delta\boldsymbol{\mathcal{S}}_{lx,i}^{\rm GS}. \tag{63}$$

As already noted, all the three iterative schemes (Jacobi, GS and SOR) involve matrix operations for the computation of the line source vector corrections (see Equations (56)

and (58)). A smart strategy to avoid such matrix computations, and thereby speed up the iterative methods, was given by Trujillo Bueno & Manso Sainz (1999). To describe this strategy in some detail, we now write the 2×2 approximate operator $\mathbf{\Lambda}_{x,ii}$ as follows:

$$\mathbf{\Lambda}_{x,ii} = \begin{pmatrix} \Lambda^{00}_{x,ii} & \Lambda^{02}_{x,ii} \\ \Lambda^{20}_{x,ii} & \Lambda^{22}_{x,ii} \end{pmatrix}, \tag{64}$$

where $\Lambda^{KK'}_{x,ii}$ are given by (see Equation (53))

$$\Lambda^{KK'}_{x,ii} = \frac{1}{2} \int_{-1}^{+1} \Psi_0^{KK'}(\mu)\, \Lambda^{KK'}_{x\mu,ii}\, \mathrm{d}\mu. \tag{65}$$

As shown by Trujillo Bueno & Manso Sainz (1999) for the CRD problem (see their Fig. 3), we also find for our PRD problem that $|\Lambda^{00}_{x,ii}| > |\Lambda^{22}_{x,ii}| \gg |\Lambda^{02}_{x,ii}| = |\Lambda^{20}_{x,ii}|$. We illustrate this fact in Fig. 7, where the elements of the monochromatic lambda matrix for a semi-infinite model atmosphere is plotted versus the line center optical depth for two different frequencies $x = 0$ (panel a) and $x = 5$ (panel b). Clearly, for $x = 0$ the elements of $\mathbf{\Lambda}_{x,ii}$ are nearly identical to that of the corresponding CRD case (compare our Fig. 7a with Fig. 3 of Trujillo Bueno & Manso Sainz 1999). As the frequency increases toward the line wing the entire curve corresponding to all the elements of this matrix shifts toward higher optical depths (see Fig. 7b). In other words, the depth at which $\Lambda^{KK'}_{x,ii}$ reaches unity, 0.7 and zero for $(K, K') = (0, 0)$, $(2, 2)$ and $(0, 2)$, respectively, shifts toward larger optical depth. This behaviour can be understood by looking at the explicit form of $\Lambda^{KK'}_{x\mu,ii}$. In the case of a short-characteristic formal solver, $\Lambda^{KK'}_{x\mu,ii} \approx \Psi_{x,O}(\mu)$, where O is the depth point of interest (here $O = i$). The quantity $\Psi_{x,O}(\mu)$ is given by

$$\Psi_{x,O}(\mu) = w_0 - \frac{(\Delta\tau_P - \Delta\tau_M)w_1 + w_2}{\Delta\tau_P \Delta\tau_M}, \tag{66}$$

with $w_0 = 1 - \exp(-\Delta\tau_M)$, $w_1 = w_0 - \Delta\tau_M \exp(-\Delta\tau_M)$ and $w_2 = 2w_1 - \Delta\tau_M^2 \exp(-\Delta\tau_M)$. Clearly, when both $\Delta\tau_M$ and $\Delta\tau_P$ tend to infinity, $\Psi_{x,O}(\mu) \to 1$, and then it is easy to see from Equations (65), (45) and (36) that $\Lambda^{KK'}_{x,ii}$ saturate to their respective values mentioned above. As x increases the optical depth at which $\Psi_{x,O}(\mu) \to 1$ shifts to larger optical depths, and hence the observed behaviour. Thus, saturation is reached when $\Psi_{x,O}(\mu) \to 1$. This is perhaps equivalent to saying that saturation is reached when the exponential in the kernel (see Equation (19) of Faurobert-Scholl et al. 1997) can be replaced reasonably well by a delta function in the grid interval around the optical depth τ_i. It is worth noting that as $\Lambda^{KK'}_{x,ii}$ depends on the optical depth grid, the finer the grid the slightly larger is the depth at which saturation is reached.

Thus, following Trujillo Bueno & Manso Sainz (1999) we can also set $\Lambda^{22}_{x,ii} = \Lambda^{02}_{x,ii} = \Lambda^{20}_{x,ii} = 0$, and still obtain a radiative transfer method with a convergence rate that is as

good as that achieved by keeping the full $\mathbf{\Lambda}_{x,ii}$ given in Equations (64) and (65) (see Fig. 4 of Trujillo Bueno & Manso Sainz 1999). The use of such a strategy leads to a decoupling of the equations for $(\delta S_{lx,i})_0^0$ and $(\delta S_{lx,i})_0^2$ as follows (see Equations (54), (50), and (64)):

$$(\delta S_{lx,i})_0^0 - \int_{-\infty}^{+\infty} (N_{xx'})_{00}\, p_{x'}\, \Lambda_{x',ii}^{00}\, (\delta S_{lx',i})_0^0\, \mathrm{d}x' = \epsilon B + (\bar{J}_{x,i}^{\mathrm{old}})_0^0 - (S_{lx,i}^{\mathrm{old}})_0^0\,, \tag{67}$$

$$(\delta S_{lx,i})_0^2 = W_2\ (\bar{J}_{x,i}^{\mathrm{old}})_0^2 - (S_{lx,i}^{\mathrm{old}})_0^2\,, \tag{68}$$

where $(N_{xx'})_{00}$ is the first diagonal element of $\mathbf{N}_{xx'}$ given in Equation (50).

In summary, the $(\delta S_{lx,i})_0^0$ correction is computed using a Jacobi, GS or SOR iteration, while the $(\delta S_{lx,i})_0^2$ correction is formally similar to the classical Λ-iteration. However, the important difference with respect to the classical Λ-iteration method is that the $(I_{x\mu,i})_0^0$ which enters the computation of $(J_{x,i})_0^2$ (see Equation (51)) is calculated with the improved $(S_{x,i})_0^0$ value that was obtained in the previous iterative step.

Finally, we remark the following two important points: (1) As in the case of unpolarized transfer, in the polarized case we again find that as long as $\Gamma_{\mathrm{E}}/\Gamma_{\mathrm{R}} < 10$ we can approximate $g_{xx'}^{\mathrm{III}}$ by $\phi_{x'}$ in the core and neglect it in the wings. But as soon as $\Gamma_{\mathrm{E}}/\Gamma_{\mathrm{R}} \geq 10$, to get the converged solution we have to approximate $g_{xx'}^{\mathrm{III}}$ by $\phi_{x'}$ throughout the line profile for the line source vector correction computation. (2) All the above-mentioned iterative schemes are given for the DH redistribution matrix. It is not difficult to apply them for the hybrid approximation (see Equation (33)). In this case we simply replace $\mathbf{N}_{xx'}$ by $(1-\epsilon)g_{xx'}^{k}\mathbf{E}$ and in Equations (58) and (59) set $\alpha = (1-\epsilon)$ and $\boldsymbol{\mathcal{B}} = (1-\epsilon)\mathbf{E}$. Furthermore, when applying CRD-CS for $k = \mathrm{I}, \mathrm{III}$ we do the same approximations as we did for unpolarized case (see § 3.1.2.).

7. The true error for $(S_x)_0^2$

In § 4 we presented a detailed study of the true error for the unpolarized PRD source function. In this section we present similar studies for $(S_x)_0^2$. We note that the behaviour of T_e, C_e and R_c presented in § 4 for the unpolarized source function is similar for $(S_x)_0^0$. Therefore, we consider only $(S_x)_0^2$ here. The results are presented in Figs. 8 and 9.

The definition of T_e, C_e and R_c for $(S_x)_0^2$ is also given by Equations (26)–(28), but with S_{lx} replaced by $(S_x)_0^2$. However, $(S_x)_0^2$ is a sign changing quantity. Thus, in the denominator of Equations (26)–(28), we need to replace S_{lx} by $|(S_x)_0^2|$. Furthermore, it is well known that in general $(S_x)_0^2$ is two orders of magnitude smaller than $(S_x)_0^0$. Therefore, we find that in our PRD case the maximum relative change R_c for $(S_x)_0^2$ reaches approximately a minimum

value of 10^{-8} and then starts to fluctuate around it. Thus, to find a fully converged solution on a given grid resolution level g, we iterate until $R_c < 10^{-8}$. We remark that we adopt the same method as described in § 4 to find the true error as well as the convergence error for $(S_x)^2_0$.

As in § 4, here we consider the hybrid approximation with $R_{\rm I,II,III,AA}$ redistribution functions and the DH redistribution matrix. Again, we consider a semi-infinite atmosphere with the lower boundary condition $(I_{x\mu})^K_0 = B\,\delta_{K0}$, and the upper boundary condition $(I_{x\mu})^K_0 = 0$ for $K = 0, 2$. A depth grid of 9 points per decade (i.e., $\Delta Z = 0.25$) and a Gaussian quadrature with 5 μ-values $[0 < \mu < 1]$ are used. The frequency grid used is exactly the same as that chosen for the unpolarized case. Other parameters are $\epsilon = 10^{-4}$, $r = 0$, $B = 1$, and $a = 10^{-3}$ for type II and type III redistribution, unless stated otherwise. We initialize all the three iterative schemes discussed in this paper by the LTE solution: $(S_{lx})^K_0 = B\,\delta_{K0}$. It is worthwhile to note that if the initial or starting solution is other than the above-mentioned LTE solution, then the true error that one obtains for a given grid resolution (after reaching the plateau region of the T_e curve) remains the same. However, the path followed to reach that T_e is different.

We find that the true error for $(S_x)^2_0$ is in general larger by one order of magnitude compared to that for $(S_x)^0_0$. Fig. 8 shows the T_e, C_e and R_c for $(S_x)^2_0$ with the hybrid approximation and $R_{\rm I,II,III,AA}$ redistribution functions. As in the unpolarized case, the true error for $(S_x)^2_0$ is the largest for the $R_{\rm II,AA}$ redistribution function case. It is about 23 %. However, as discussed for the unpolarized case, addition of the continuum or inclusion of elastic collisions through the use of the DH redistribution matrix improves the true error significantly. For example, the true error for $(S_x)^2_0$ is approximately 2.3 % for $\Gamma_{\rm E}/\Gamma_{\rm R} = 1$ (see the bottom solid line in Fig. 9) without continuum, and it is 1 % for $\Gamma_{\rm E}/\Gamma_{\rm R} = 0$ and $r = 10^{-4}$ (figure not shown).

8. Conclusions

In this paper we have shown how to solve efficiently and accurately the non-LTE resonance line formation problem in stellar atmospheres, taking into account PRD effects with and without scattering polarization. To this end, we have generalized the Gauss-Seidel (GS) and Successive Over-Relaxation (SOR) radiative transfer methods that Trujillo Bueno & Fabiani Bendicho (1995) and Trujillo Bueno & Manso Sainz (1999) developed for solving unpolarized and polarized CRD problems, respectively. These iterative methods are based on the concept of operator splitting. As in the CRD case, we find that these methods are superior to the Jacobi-based ALI method. Quantitatively, the symmetric GS method (SYM-GS) is 4 times faster

than Jacobi, while the symmetric SOR method (SSOR) is about 10 times faster without the need of refining the choice of the ω-parameter. We emphasize that our implementation of these highly convergent radiative transfer methods do not require neither the construction nor the inversion of any non-local Λ-operator, so that the computing time per iteration is similar to that of the Jacobi method. Therefore, these GS-based methods are suitable also for the solution of non-LTE problems in three-dimensional model atmospheres.

For the unpolarized PRD problem, we have considered the case of pure Doppler redistribution (type I), Doppler, natural and collisionally broadened type III redistribution, Doppler and naturally broadened type II redistribution, and a combined case of type II and type III redistribution. For the PRD problem of resonance line polarization we have considered both the hybrid approximation with angle-averaged type I, II and III redistribution functions and the general redistribution matrix of Domke & Hubeny (1988) that properly takes into account the elastic and depolarizing collisions. The methods we have developed here can be used also for solving the resonance line polarization problem in the presence of a magnetic field that does not break the axial symmetry of the problem. For the case of a weak magnetic field with a given strength, inclination and azimuth at each spatial grid point the corresponding redistribution matrices are substantially more complicated (e.g., Bommier 1997), but the generalization of the same GS-based methods is straightforward in spite of the fact that the number of unknowns is three times larger.

Finally, we emphasize that the PRD radiative transfer problem we have considered here is that of a two-level model atom without the possibility of lower-level polarization, which implies that it is assumed that only the emission term of the transfer equation contributes to scattering polarization. Fortunately, there are several diagnostically important resonance lines for which this two-level atom approximation is probably suitable (e.g., the k line of Mg II). In forthcoming papers we will show how the application of the computer programs described here allow us to gain physical insight and to make predictions on the Q/I shapes produced by PRD effects.

Financial support by the Spanish Ministry of Science and Innovation through projects AYA2007-63881 (Solar Magnetism and High-Precision Spectropolarimetry) and CONSOLIDER INGENIO CSD2009-00038 (Molecular Astrophysics: The Herschel and Alma Era) is gratefully acknowledged. We are also grateful to the referee for carefully reviewing our paper.

REFERENCES

Anusha, L. S., Nagendra, K. N., Paletou, F., & Léger, L. 2009, ApJ, 704, 661

Asensio Ramos, A., & Trujillo Bueno, J. 2006, in EAS Publication Series 18, Radiative Transfer and Applications to Very Large Telescopes, ed. Ph. Stee (EAS, EDP Sciences) 25

Auer, L. 1987, in Numerical Radiative Transfer, ed. W. Kalkofen (Cambridge: Cambridge Univ. Press), 101

Auer, L. 1991, in Stellar Atmospheres: Beyond Classical Models, ed. L. Crivellari, I. Hubeny, & D. G. Hummer (Dordrecht: Kluwer), 9

Auer, L., Fabiani Bendicho, P., & Trujillo Bueno, J. 1994, A&A, 292, 599

Auer, L., & Paletou, F. 1994, A&A, 285, 675

Belluzzi, L., & Landi Degl'Innocenti, E. 2009, A&A, 495, 577

Bommier, V. 1997, A&A, 328, 726

Cannon, C. J. 1973, ApJ, 185, 621

Cannon, C. J. 1985, The transfer of spectral line radiation (Cambridge: Cambridge University Press)

Castor, J. 2004, Radiation Hydrodynamics (Cambridge University Press)

Chandrasekhar, S. 1950, Radiative transfer (Oxford: Clarendon Press)

Chevallier, L., Paletou, F., & Rutily, B. 2003, A&A, 411, 221

Domke, H., & Hubeny, I. 1988, ApJ, 334, 527

Fabiani Bendicho, P., & Trujillo Bueno, J. 1999, in Solar Polarization, ed. K. N. Nagendra, & J. O. Stenflo (Boston: Kluwer), 219

Fabiani Bendicho, P., Trujillo Bueno, J., & Auer, L. 1997, A&A, 324, 161

Faurobert, M. 1987, A&A, 178, 269

Faurobert, M. 1988, A&A, 194, 268

Faurobert-Scholl, M., 1992, A&A, 258, 521

Faurobert-Scholl, M., 1993, A&A, 268, 765

Faurobert-Scholl, M., Frisch, H., & Nagendra, K. N. 1997, A&A, 322, 896

Feautrier, P. 1964, C. R. Acad. Sci. Paris, 258, 3189

Fluri, D. M., Nagendra, K. N., & Frisch, H. 2003, A&A, 400, 303

Frisch, H. 1980, A&A, 83, 166

Frisch, H. 1988, in Radiation in moving gaseous media, ed. Y. Chmielewski, & T. Lanz (Switzerland: Geneva Observatory), 337

Frisch, H. 2007, A&A, 476, 665

Frisch, H., Anusha, L. S., Sampoorna, M., & Nagendra, K. N. 2009, A&A, 501, 335

Gandorfer, A. 2000, The Second Solar Spectrum, Vol I: 4625 Å to 6995 Å (Zurich: vdf Hochschulverlag)

Gandorfer, A. 2002, The Second Solar Spectrum, Vol II: 3910 Å to 4630 Å (Zurich: vdf Hochschulverlag)

Gandorfer, A. 2005, The Second Solar Spectrum, Vol III: 3160 Å to 3915 Å (Zurich: vdf Hochschulverlag)

Heinzel, P. 1981, J. Quant. Spec. Radiat. Transf., 25, 483

Hubeny, I. 2003, in ASP Conf. Ser. 288, Stellar Atmosphere Modeling, ed. I. Hubeny, D. Mihalas, & K. Werner (San Francisco: ASP), 17

Hummer, D. G. 1962, MNRAS, 125, 21

Ivanov, V. V. 1995, A&A, 303, 609

Klein, R. I., Castor, J. I., Greenbaum, A., Taylor, D., & Dykema, P. G. 1989, J. Quant. Spec. Radiat. Transf., 41, 199

Kunasz, P., & Auer, L. H. 1988, J. Quant. Spec. Radiat. Transf., 39, 67

Landi Degl'Innocenti, E. 1984, Sol. Phys., 91, 1

Landi Degl'Innocenti, E., & Landolfi, M. 2004, Polarization in spectral lines (Dordrecht: Kluwer)

Manso Sainz, R., & Trujillo Bueno, J. 1999, in Solar Polarization, ed. K. N. Nagendra, & J. O. Stenflo (Boston: Kluwer), 143

Manso Sainz, R., & Trujillo Bueno, J. 2003, in ASP Conf. Ser. 307, Solar Polarization, ed. J. Trujillo Bueno, & J. Sánchez Almeida (San Francisco: ASP), 251

McKenna, S. J. 1984, Ap&SS, 106, 283

Mihalas, D. 1978, Stellar atmosphere (2nd ed.; San Francisco: Freeman)

Nagendra, K. N. 1986, PhDT, Radiative transfer with Stokes vector (Bangalore: Bangalore University)

Nagendra, K. N. 1988, ApJ, 335, 269

Nagendra, K. N. 1989, Ap&SS, 154, 119

Nagendra, K. N. 1994, ApJ, 432, 274

Nagendra, K. N. 1995, Ap&SS, 274, 523

Nagendra, K. N. 2003, in ASP Conf. Ser. 288, Stellar Atmosphere Modeling, ed. I. Hubeny, D. Mihalas, & K. Werner (San Francisco: ASP), 583

Nagendra, K. N., Anusha, L. S., & Sampoorna, M. 2009, Mem. Soc. Astron. Italiana, 80, 678

Nagendra, K. N., Frisch, H., & Faurobert-Scholl, M. 1998, A&A, 332, 610

Nagendra, K. N., Paletou, F., Frisch, H., & Faurobert-Scholl, M. 1999, in Solar Polarization, ed. K. N. Nagendra, & J. O. Stenflo (Boston: Kluwer), 127

Nagendra, K. N., & Sampoorna, M. 2009, in ASP Conf. Ser. 405, Solar Polarization 5, ed. S. V. Berdyugina, K. N. Nagendra, & R. Ramelli (San Francisco: ASP), 261

Olson, G. L., Auer, L. H., & Buchler, J. R. 1986, J. Quant. Spec. Radiat. Transf., 35, 431

Omont, A., Smith, E. W., & Cooper, J. 1972, ApJ, 175, 185

Oxenius, J., & Simonneau, E. 1994, Annals of Physics, 234, 60

Paletou, F., & Anterrieu, E. 2009, A&A, 507, 1815

Paletou, F., & Auer, L. H. 1995, A&A, 297, 771 (PA95)

Paletou, F., & Faurobert-Scholl, M. 1997, A&A, 328, 343

Rees, D. E., & Saliba, G. J. 1982, A&A, 115, 1

Sampoorna, M., Nagendra, K. N., & Frisch, H. 2008, J. Quant. Spec. Radiat. Transf., 109, 2349

Scharmer, G. B. 1983, A&A, 117, 83

Stenflo, J. O. 1994, Solar magnetic fields - Polarized radiation diagnostics (Dordrecht: Kluwer)

Stenflo, J. O., & Keller, C. U. 1997, A&A, 321, 927

Trujillo Bueno, J. 1999, in Solar Polarization, ed. K. N. Nagendra, & J. O. Stenflo (Boston: Kluwer), 73

Trujillo Bueno, J. 2003, in ASP Conf. Ser. 288, Stellar atmosphere modeling, eds. I. Hubeny, D. Mihalas, & K. Werner (San Francisco: ASP), 551

Trujillo Bueno, J. 2009, in ASP Conf. Ser. 405, Solar Polarization 5, ed. S. V. Berdyugina, K. N. Nagendra, & R. Ramelli (San Francisco: ASP), 65

Trujillo Bueno, J., & Fabiani Bendicho, P. 1995, ApJ, 455, 646 (TF95)

Trujillo Bueno, J., & Landi Degl'Innocenti, E. 1996, Sol. Phys., 164, 135

Trujillo Bueno, J., & Manso Sainz, R. 1999, ApJ, 516, 436

Uitenbroek, H. 2001, ApJ, 557, 389

Vardavas, I. M., & Cannon, C. J. 1976, A&A, 53, 107

Vinsome, P. K. W. 1976, in Proc. 4th Symp. on Numerical Simulation of Reservoir Performance of SPE of AIME, 140

Table 1. The true error in the case of type II redistribution for different resolutions of the depth grid. For all cases, $\epsilon = 10^{-4}$, $a = 10^{-3}$ and $r = 0$.

ΔZ	Number of points per decade	T_e
0.5	4.5	0.2571
0.25	9	0.1244
0.125	18	0.0638
0.1	23	0.0533
0.04	28.75	0.0238
0.02	57.5	0.0130
0.01	115	0.0069

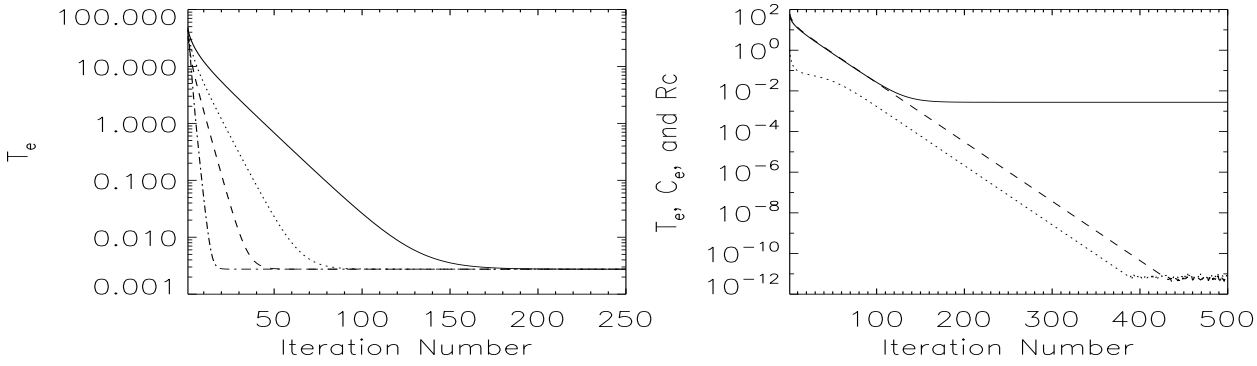

Fig. 1.— Pure Doppler (type I) redistribution. Convergence properties of the various iterative schemes in a semi-infinite isothermal model atmosphere with $\epsilon = 10^{-4}$ and a spatial grid with 9 points per decade ($\Delta Z = 0.25$). Left panel: solid line (Jacobi), dotted line (GS), dashed line (SYM-GS), dot-dashed line (SSOR, $\omega_{\rm opt} = 1.6$). Right panel: solid line (T_e), dotted line (R_c), and dashed line (C_e), are computed using the Jacobi iterative scheme.

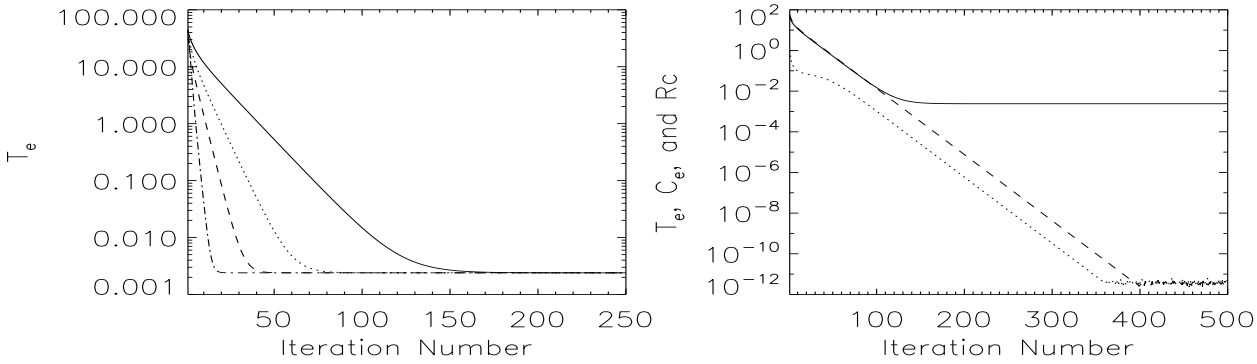

Fig. 2.— Doppler, natural and collisional (type III) redistribution. Convergence properties of the various iterative schemes in a semi-infinite isothermal model atmosphere with $\epsilon = 10^{-4}$, $a = 10^{-3}$ and a spatial grid with 9 points per decade ($\Delta Z = 0.25$). The different line types are the same as in Fig. 1.

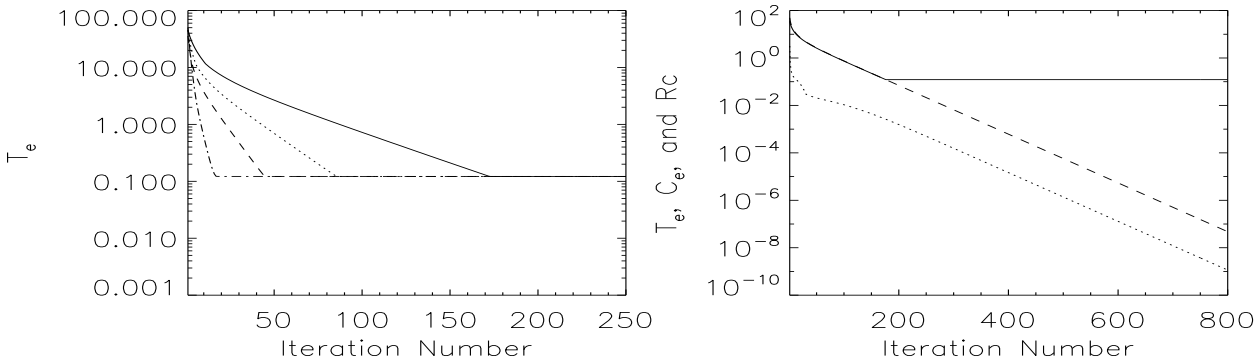

Fig. 3.— Doppler and natural broadening (type II redistribution). Convergence properties of the various iterative schemes in a semi-infinite isothermal model atmosphere with $\epsilon = 10^{-4}$, $a = 10^{-3}$ and a spatial grid with 9 points per decade ($\Delta Z = 0.25$). The line types and the model parameters are exactly the same as in Fig. 2.

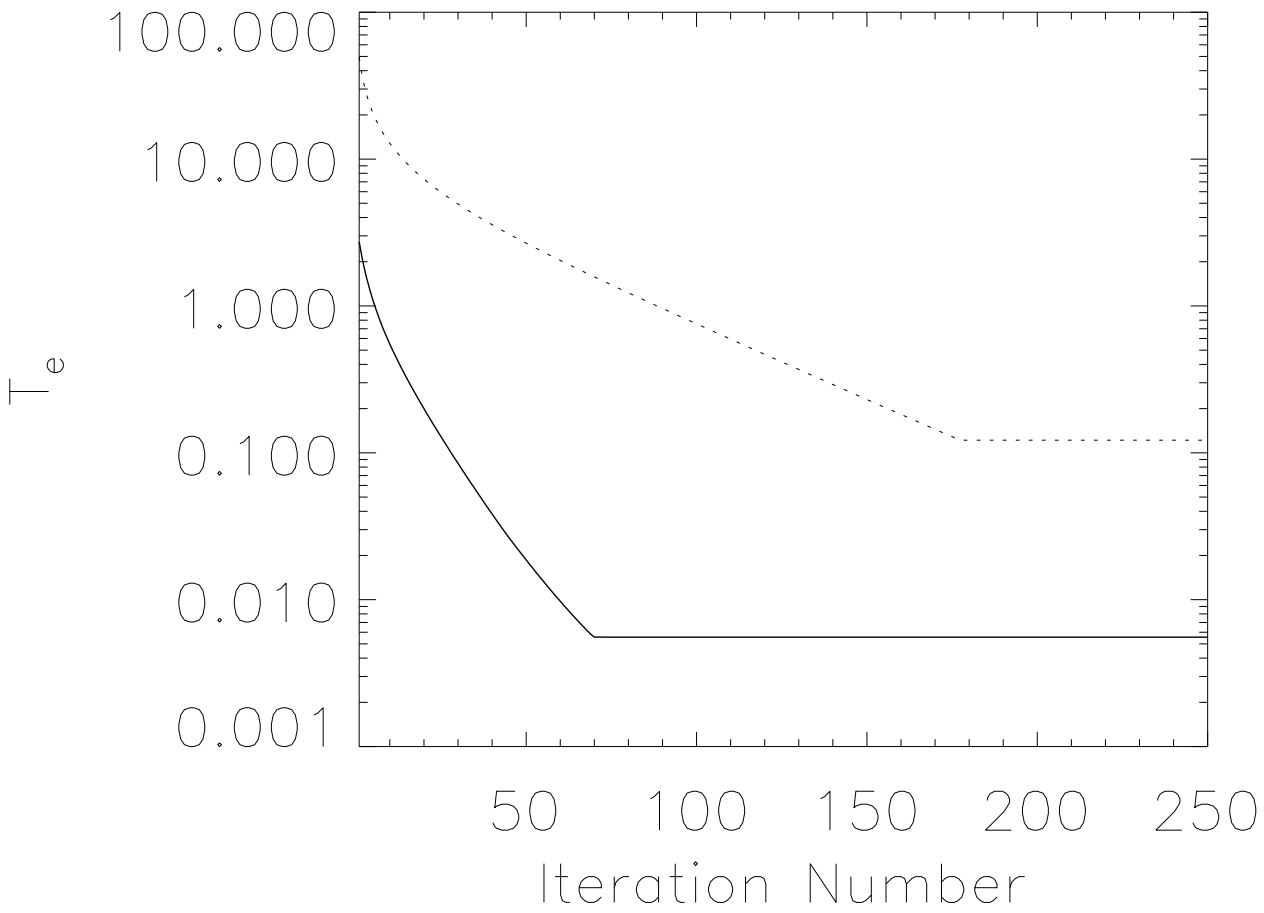

Fig. 4.— Study of the true error for the type II redistribution function problem. Different line types: solid line ($\epsilon = 10^{-2}$), and dotted line ($\epsilon = 10^{-4}$). A semi-infinite isothermal model atmosphere with $a = 10^{-3}$ and a spatial grid with 9 points per decade ($\Delta Z = 0.25$) are used.

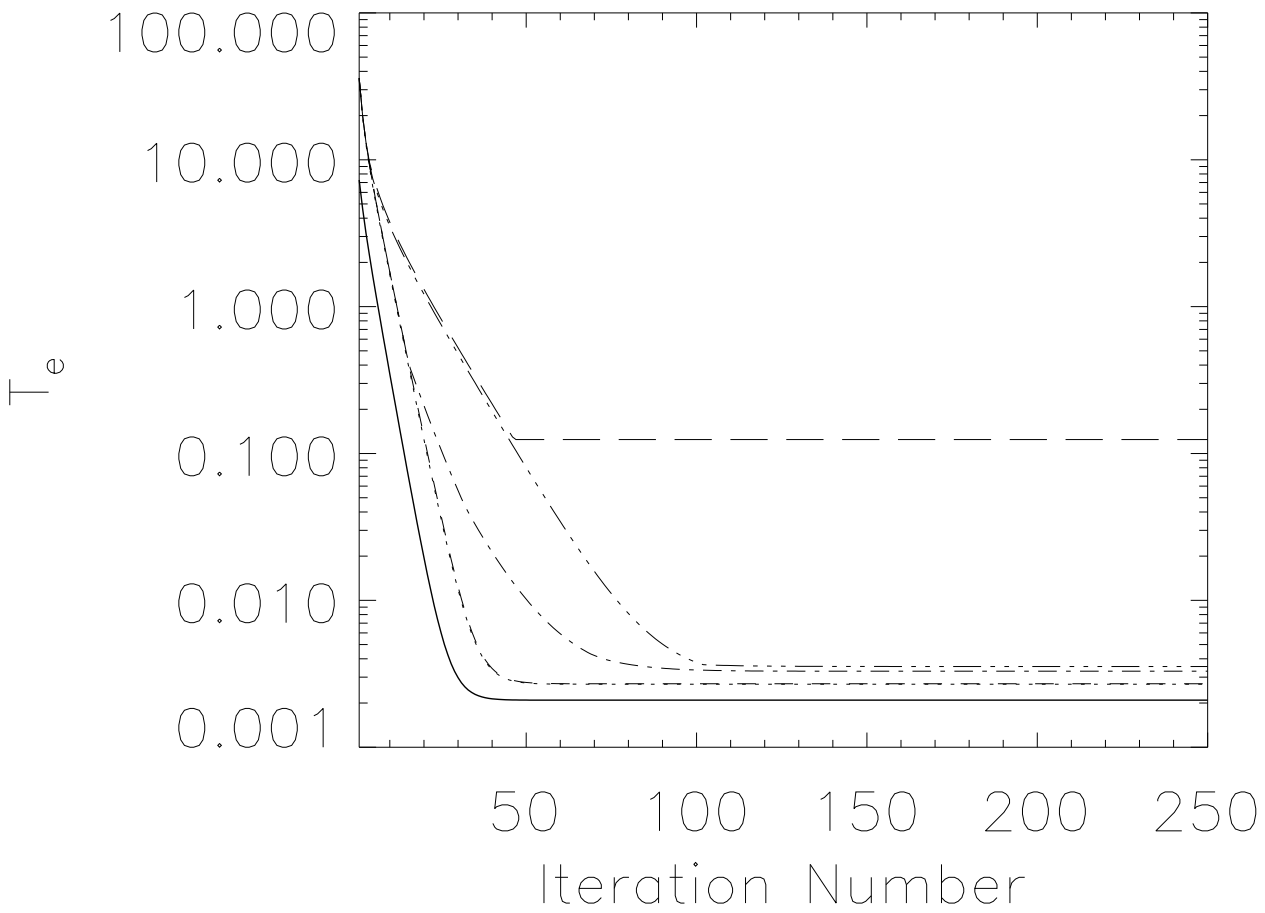

Fig. 5.— Study of the true error for the type II redistribution function case. Effect of the continuum parameter r. The non-LTE parameter $\epsilon = 10^{-4}$ and the depth grid spacing $\Delta Z = 0.25$. Solid line: $r = 10^{-4}$, dotted line: $r = 10^{-6}$, dashed line: $r = 10^{-8}$, dot-dashed line: $r = 10^{-10}$, dash-triple-dotted line: $r = 10^{-12}$, and long-dashed line: $r = 0$. Note that the dotted and dashed lines merge to give a dot-dashed line.

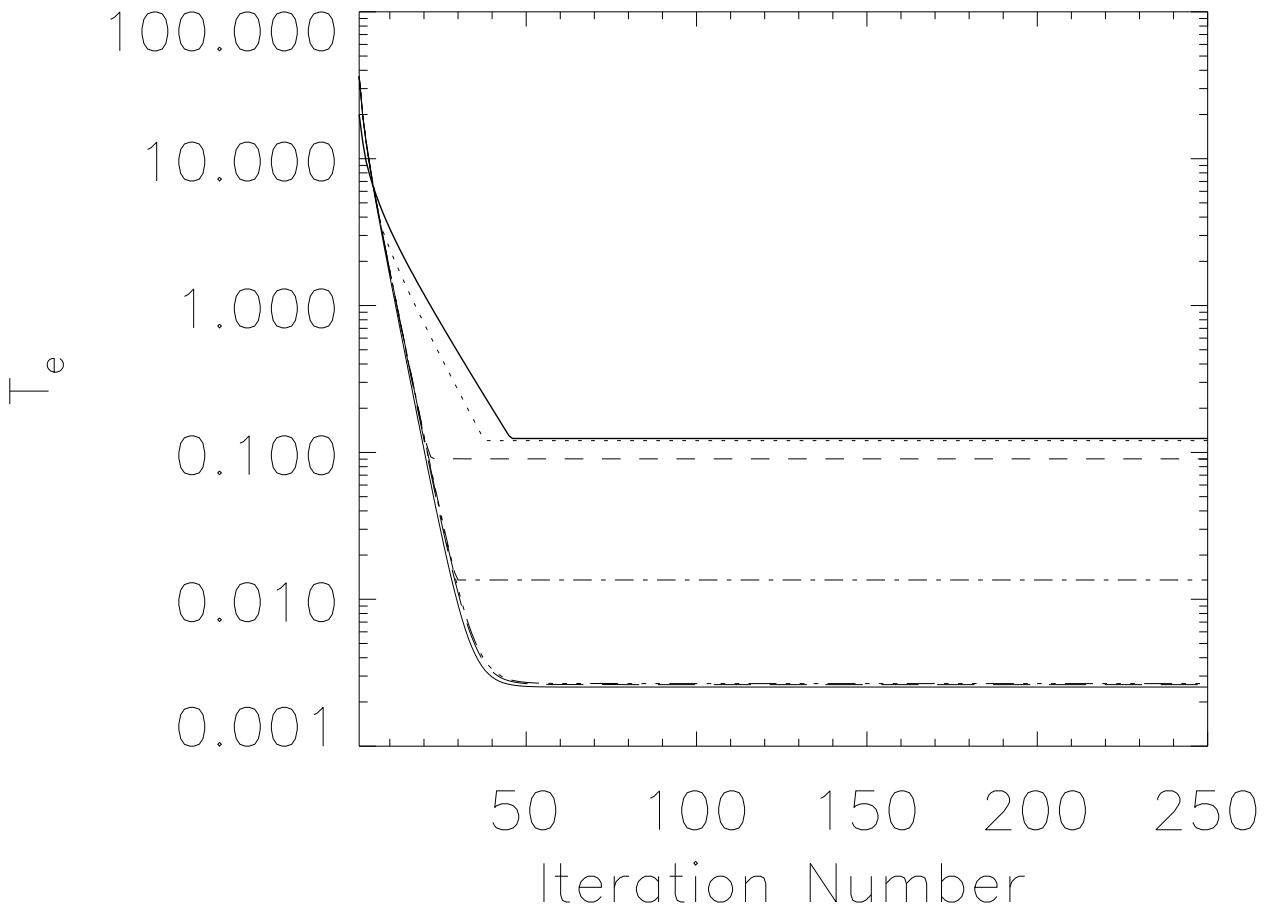

Fig. 6.— Study of the true error for the combined case of type II and III redistribution function. Effect of the elastic collision parameter $\Gamma_{\rm E}/\Gamma_{\rm R}$. The non-LTE parameter $\epsilon = 10^{-4}$, the continuum parameter $r = 0$ and the depth grid spacing $\Delta Z = 0.25$. The topmost solid line: $\Gamma_{\rm E}/\Gamma_{\rm R} = 0$, dotted line: $\Gamma_{\rm E}/\Gamma_{\rm R} = 10^{-4}$, dashed line: $\Gamma_{\rm E}/\Gamma_{\rm R} = 10^{-3}$, dot-dashed line: $\Gamma_{\rm E}/\Gamma_{\rm R} = 10^{-2}$, dash-triple-dotted line: $\Gamma_{\rm E}/\Gamma_{\rm R} = 0.1$, long-dashed line: $\Gamma_{\rm E}/\Gamma_{\rm R} = 0.25$, and the bottom most solid line: $\Gamma_{\rm E}/\Gamma_{\rm R} = 1$.

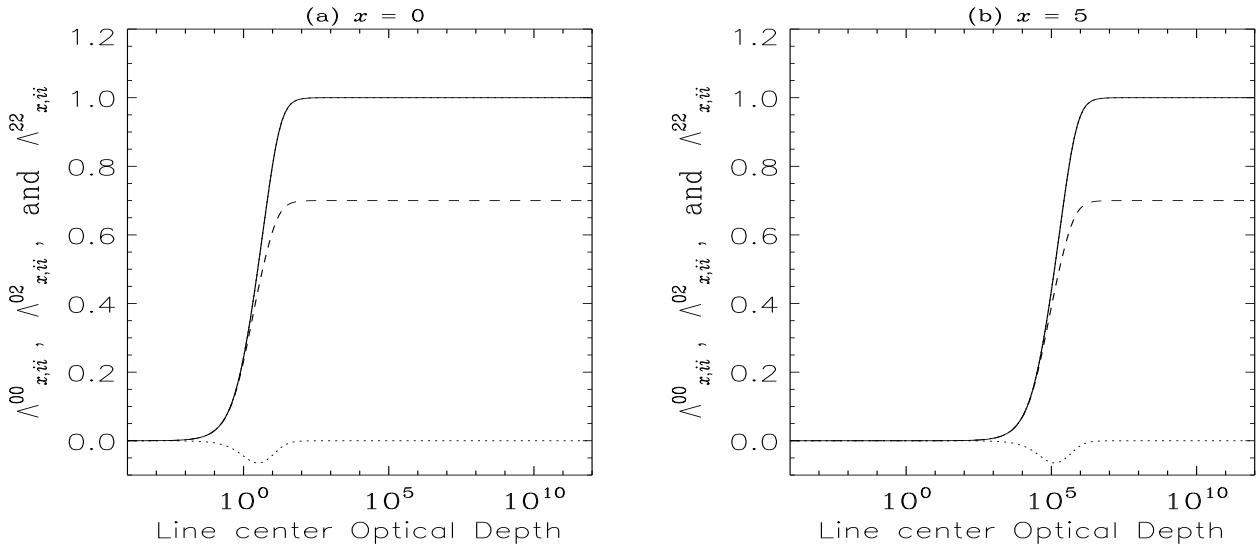

Fig. 7.— Variation of the diagonal elements of the monochromatic lambda operator with the line center optical depth. A semi-infinite model atmosphere with no continuum ($r = 0$) and damping parameter $a = 10^{-3}$ are used. The solid line corresponds to $\Lambda^{00}_{x,ii}$, the dotted line to $\Lambda^{02}_{x,ii}$ and the dashed line to $\Lambda^{22}_{x,ii}$.

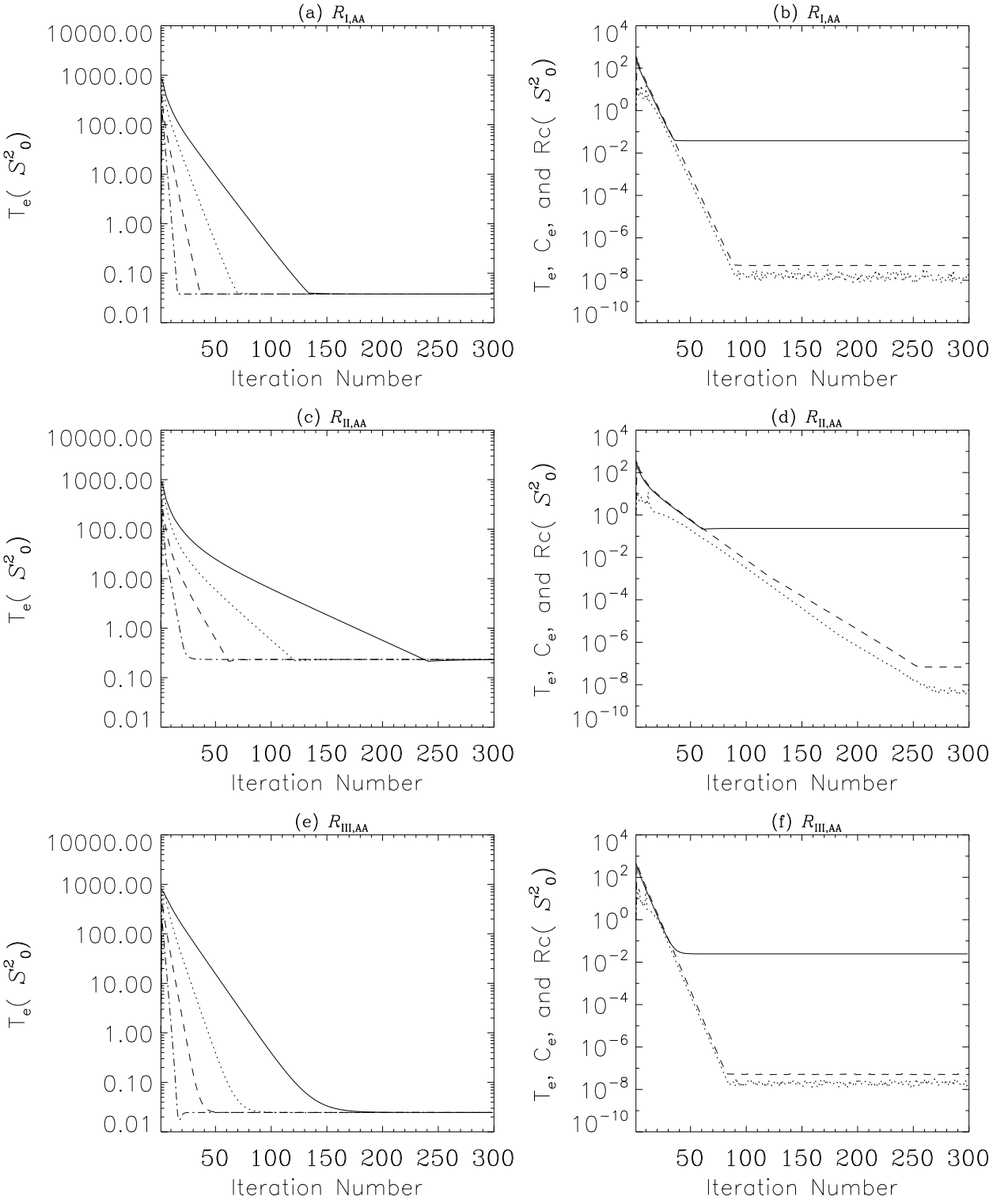

Fig. 8.— T_e, C_e and R_c for $(S_x)^2_0$. Convergence properties of the various iterative schemes. Left panels: solid line (Jacobi), dotted line (GS), dashed line (SYM-GS), dot-dashed line (SSOR, $\omega_{\rm opt} = 1.6$). Right panels: solid line (T_e), dotted line (R_c), and dashed line (C_e), computed using the SYM-GS iterative scheme. For type II and type III redistribution the damping parameter $a = 10^{-3}$. A spatial grid with 9 points per decade ($\Delta Z = 0.25$) is used.

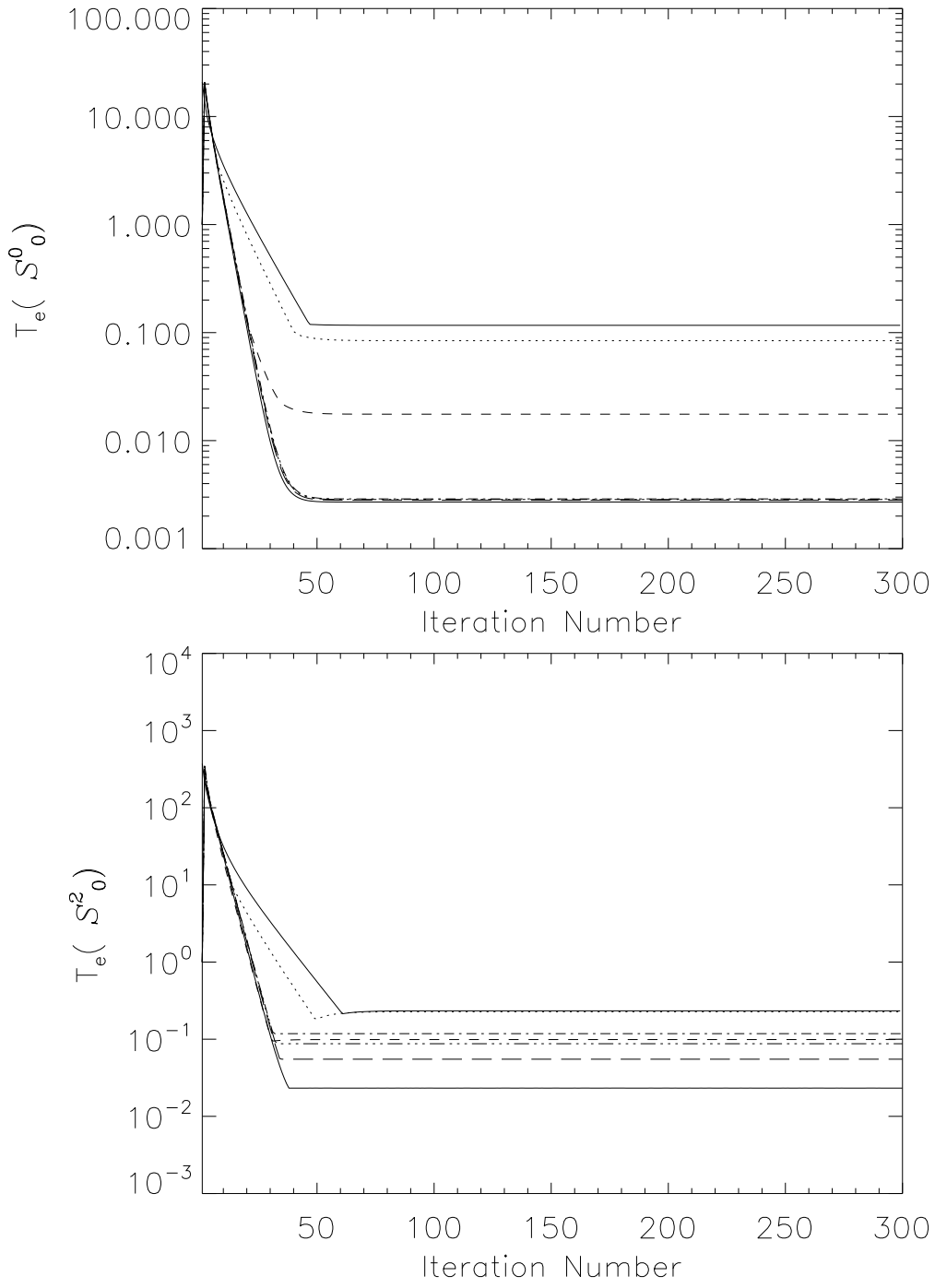

Fig. 9.— True error for the DH redistribution function problem. Effect of the elastic collision parameter $\Gamma_{\rm E}/\Gamma_{\rm R}$. The non-LTE parameter $\epsilon = 10^{-4}$, the damping parameter $a = 10^{-3}$, $r = 0$ (pure line case), $D^{(2)} = 0.5\,\Gamma_{\rm E}$, and depth grid spacing $\Delta Z = 0.25$. The topmost solid line: $\Gamma_{\rm E}/\Gamma_{\rm R} = 0$, dotted line: $\Gamma_{\rm E}/\Gamma_{\rm R} = 10^{-4}$, dashed line: $\Gamma_{\rm E}/\Gamma_{\rm R} = 10^{-3}$, dot-dashed line: $\Gamma_{\rm E}/\Gamma_{\rm R} = 10^{-2}$, dash-triple-dotted line: $\Gamma_{\rm E}/\Gamma_{\rm R} = 0.1$, long-dashed line: $\Gamma_{\rm E}/\Gamma_{\rm R} = 0.25$, and the bottom solid line: $\Gamma_{\rm E}/\Gamma_{\rm R} = 1$.